

# DUAL-MODALITY SMALL ANIMAL IMAGING

A thesis submitted in partial fulfillment of the requirement  
for the degree of Bachelor of Science with Honors in Physics  
from the College of William and Mary in Virginia,

by

Amoreena Elizabeth Ranck

Accepted for \_\_\_\_\_

(Honors, High Honors, or Highest Honors)

---

Dr. Robert Welsh

---

Dr. Keith Griffioen

---

Dr. Dennis Manos

---

Dr. Eric Bradley

Williamsburg, VA  
May 2001

## ACKNOWLEDGEMENTS

I would first like to thank Dr. Bob Welsh, my advisor, for his countless hours of work and encouragement; Dr. Eric Bradley who, among his many biology students, took time to talk about biology to a physics student; and especially Drs. Dennis Manos, David Armstrong, and Marc Sher for reminding me why I wanted to study physics in the first place.

To Remi Howell, for his support and patience; Alicia Ranck, who in spite of being my sister is still one of my best friends; my parents are responsible for making me who I am today; Will McBride, Greg Jones, and Leah Johnson who spent hours of our lives spent together working on problem sets; and finally, to those who have been there for me through everything, I could not have done this without you.

I would like to thank the Jefferson Lab detector group, especially Drew Weisenberger for their expertise and problem solving that would have taken me months longer. I must also acknowledge ORAU for their support during the summer of 2000 through the Energy Research Undergraduate Lab Fellowship and the Howard Hughes Medical Institute for their Student Travel Grant, which allowed me to present this research at the SESAPS conference in Mississippi in November 2000 and the Small Reasearch Grant which aided with the purchase of a digital camera for the system.

## LIST OF FIGURES

Figure 1. Electronic band structure of inorganic crystals.....	9
Figure 2. Parallel-hole collimator geometry.....	10
Figure 3. Pinhole collimator geometry.....	11
Figure 4. Position-sensitive photomultiplier tube.....	12
Figure 5. The decay of $^{125}\text{I}$ .....	13
Figure 6. Gamma image.....	15
Figure 7. X-ray image.....	15
Figure 8. Composite image.....	16
Figure 9. Lixi Fluoroscope.....	17
Figure 10. PSPMT setup.....	20
Figure 11. Electronics.....	23
Figure 12. Mouse bed.....	25
Figure 13. Data Acquisition user interface.....	26
Figure 14. Time Cuts program user interface.....	27
Figure 15. Data Analysis user interface.....	28
Figure 16. Comparison of injection sites.....	32
Figure 17. SZT vs. control mouse.....	33
Figure 18. Low count rate region.....	34
Figure 17. Comparison of pinhole to parallel-hole collimated images.....	34
Figure 18. Gantry.....	35
Figure 19. M-64 PSPMT.....	37

## TABLE OF CONTENTS

<b>Acknowledgements.....</b>	<b>ii</b>
<b>List of Figures.....</b>	<b>iii</b>
<b>Abstract.....</b>	<b>v</b>
<b>I. Introduction.....</b>	<b>1</b>
<b>II. Biology Background.....</b>	<b>3</b>
A. Biological Imaging.....	3
B. Tagged Ligands.....	4
C. Diabetes.....	4
<b>III. Physics Background.....</b>	<b>5</b>
A. Imaging Methods.....	5
B. Detectors.....	8
1. <i>Scintillators</i> .....	8
2. <i>Collimators</i> .....	9
3. <i>Photomultiplier Tubes</i> .....	11
C. $^{125}\text{I}$ .....	12
<b>IV. Dual-Modality.....</b>	<b>14</b>
A. Structural Information.....	14
B. Implementation.....	16
C. Co-registration.....	18
<b>V. System Details.....</b>	<b>20</b>
A. Gamma Detectors.....	20
B. Electronics.....	22
C. X-ray.....	23
D. Mouse Bed.....	24
<b>VI. Data Analysis.....</b>	<b>26</b>
A. Time Cuts.....	26
B. Regions of Interest.....	27
C. SPECT.....	29

<b>VII. Diabetes Studies.....</b>	<b>30</b>
A. Procedure.....	30
B. Current Results.....	31
<b>VIII. Future Improvements.....</b>	<b>35</b>
A. Rotating Gantry.....	35
B. M-64s.....	36
C. Software.....	37
D. Statistics.....	37
<b>IX. Conclusions.....</b>	<b>39</b>
<b>Appendix: Instruction Manual.....</b>	<b>40</b>
A. Data Acquisition.....	40
B. Data Analysis.....	48
C. Making Composites.....	52

## ABSTRACT

An existing detector system developed by William and Mary in conjunction with Jefferson Lab for real time *in vivo* imaging of small animals has been enhanced to include two imaging modalities. Position-sensitive photomultiplier tubes (PSPMTs) are used in conjunction with a small fluoroscopic x-ray system to provide more accurate information. The PSPMTs allow one to follow the kinetic activity of commercially available compounds labeled with  $^{125}\text{I}$  when injected into a small animal. The x-ray provides an image with useful structural information about the animal. Using small fiducial markers that appear on both the gamma and x-ray images, the two can be co-registered. The PSPMTs are coupled to CAMAC electronics and a personal computer for data acquisition and analysis. The system has most recently been used to study insulin uptake in diabetic mice. Current preliminary results are discussed along with future developments which include the incorporation a rotating gantry for Single-Photon Emission Computed Tomography (SPECT) support and the use of smaller PSPMTs.

## I. INTRODUCTION

In order to investigate disease and biological processes, accuracy is vital. Recent improvements to imaging techniques have enhanced the capabilities for diagnosis and investigation [1]. Although the field of biological imaging is not a new one, the demands for small animal imaging have recently changed. There is a growing interest in high resolution imaging to study accurately the biodistribution of radioactively labeled compounds in small animals [2]. Developing such a system that can be reasonably afforded by a small biology laboratory is among the goals of our current project. This system is modular and comprised of components that are relatively inexpensive. In addition, the choice of the radioisotope imaged,  $^{125}\text{I}$ , allows for its use in a lab that does not have on-site cyclotron facilities.

Among the new demands on small animal imaging is a trend toward more humane techniques. Researchers are working to improve experimental design while at the same time reducing the number of laboratory animals needed and minimizing the animals' pain and suffering [3]. The system being developed at William and Mary follows this new trend. By allowing imaging of small animals *in vivo*, fewer are needed. In addition, the ability to follow the distribution of the radioisotope in real time provides a researcher valuable information that would otherwise be lost.

Another advantage of the system is its data acquisition. Data are acquired event by event and stored in files that can subsequently be analyzed repeatedly to create images of different time intervals. The data are also displayed in real time, allowing for the discovery of previously unanticipated effects.

This system has been tested recently through several different studies. These have been the research of Profs. Eric Bradley and Margaret Saha of the William and Mary Biology Department. In 1999-2000, a study with the cocaine analog RTI-55 was conducted. Recently a study of diabetes was initiated with radiolabeled insulin. The earlier studies showed the need for accurate structural information about the animal being imaged. To provide useful anatomical references, an x-ray device has been incorporated into the system, allowing for dual-modality imaging. Small metal washers have been filled with plaster-of-paris which has subsequently been soaked in Na[<sup>125</sup>I]. The washers produce small dark circles on the x-ray image and small bright spots on the gamma image. The two images can then be aligned using commercial software.

Further improvements to the system are planned and have begun to be implemented. These include the incorporation of a rotating gantry to support the PSPMTs and the x-ray, at the same time allowing for three-dimensional tomography. Smaller 1 inch PSPMTs are planned to be used both in conjunction with and in place of the current 5 inch detectors.

Since this project is interdisciplinary in nature, both biology and physics backgrounds are necessary.

## II. BIOLOGY BACKGROUND

### A. Biological Imaging

The biodistribution of a compound depends on both the metabolism of the animal being studied as well as the biological function of that compound. The uptake rate gathered by following the biodistribution can give valuable information to a researcher. Depending on the compound used, imaging can be useful for many different kinds of studies. The most useful imaging techniques now being investigated utilize various forms of radiation and luminescence.

In response to increasing demands, *in vivo* methods with better accuracy and higher resolution are being developed. These methods have several advantages over the older *in vitro* techniques such as autoradiography. Since the animal being studied does not have to be sacrificed, fewer are needed. In addition, the distribution of a compound can be followed in the same animal over a length of time, instead of giving only a snapshot [4]. Since individual animals can have different responses to any given compound, this gives a more accurate picture of the progression of a distribution. Neuroreceptors, in particular, require *in vivo* techniques to accurately determine their response to radiopharmaceuticals [5].

For one technique being developed, a microbe engineered to express the luciferase gene can be injected into an animal and then followed by the bioluminescence produced. This technique is currently being explored as an alternative to the current mouse thigh model for antibiotic testing [6]. Another technique splices a fluorescent reporter gene to specific promoter genes in stem cells. When the promoter gene is

activated, the cells express a green fluorescent protein. This method is used on organ-specific genes to look for subtle chemical effects that might cause birth defects [6].

## B. Tagged Ligands

This project is based on imaging techniques that detect radioisotopes attached to biological compounds. This method relies on the fact that the chemical properties of a given element and its isotopes are identical. Therefore, the distribution of a compound bound to a radioisotope can be traced and can thus reveal information about the normal compound. Such compounds are said to be “tagged” or “labeled” [7]. Ligands, molecules that bind to specific sites on larger molecules such as proteins [8], when radioactively labeled, are particularly useful for following molecular changes in an active biological system.

In response to the increased interest in biological imaging of tagged ligands, the availability and diversity of radiopharmaceuticals has increased [9]. Some of the common labels include radioisotopes of iodine, phosphorous, technetium, sodium, sulfur, calcium, hydrogen, and carbon. Radiopharmaceutical companies now offer hundreds of compounds useful for a wide variety of studies, many of which use  $^{125}\text{I}$  as the tracer element.

## C. Diabetes

The current study at William and Mary involves the study of diabetic mice. Diabetes mellitus is a disease involving carbohydrate, protein, and fat metabolisms and relates to insufficient insulin production or increased insulin resistance. Type I diabetes,

also known as insulin dependent, is believed to result from the destruction of  $\beta$ -cells in the pancreas which produce insulin and to be caused by genetic factors triggered by environmental factors. Without insulin, a dependent individual would be susceptible to spontaneous ketosis, coma, and death. Type II diabetes, also known as non-insulin dependent, is most often caused by obesity which results in or exacerbates insulin resistance. Insulin is not required to prevent ketosis, but can be used to control hyperglycemia if diet alone cannot [10].

The mice used in the study are treated with either streptozotocin (SZT) or a high-fat diet to induce diabetes. Streptozotocin induces hyperglycemia by destroying  $\beta$ -cells in the pancreas [11]. Unlike natural diabetes, the  $\beta$ -cells can rejuvenate after treatment has stopped. A high-fat diet leads to obesity, which can increase cellular resistance to insulin.

The three ligands proposed for the diabetes study are insulin, TNF- $\alpha$  and leptin. Insulin is a hormone that is normally produced by the body. When it binds to the insulin receptor on a cell, it initiates a reaction in that cell which induces the movement of specific proteins to the cell's surface. These proteins promote the cell's acquisition of nutrients, including glucose [12]. Tumor necrosis factor- $\alpha$  (TNF- $\alpha$ ) suppresses cell division [13]. TNF- $\alpha$  can be found in fat tissue and when produced at high levels can result in the body's resistance to insulin. Leptin is another protein found in fat tissue, but can lead to obesity and diabetes when found in unusually low levels [14].

### **III. PHYSICS BACKGROUND**

#### **A. Imaging Methods**

Many different imaging techniques have been developed to study biological processes in both humans and animals. Physical, structural, and functional information can be gathered using different imaging modalities. These techniques are often classified by the type of energy used and the way it interacts with biological tissue [15].

Ultrasound Imaging provides information about the internal structure of the body by the interaction of sonic waves with tissues. These sonic waves are either transmitted or reflected depending on the properties of the tissues being imaged [15]. Other types of imaging also exploit the specific properties of various tissues. Nuclear Magnetic Resonance (NMR), called Magnetic Resonance Imaging (MRI) when used for medical diagnosis, relies on the fact that a nucleus can be in one of two spin states. When a nucleus is placed in a magnetic field, it begins to precess with a specific frequency. By applying electromagnetic radiation of the same frequency, a nucleus with the lower energy spin state can flip to the higher energy spin state. NMR measures the characteristic relaxation time, how long it takes for a nucleus to return to its ground state. In the body, hydrogen (usually in water), triglycerides, and membrane phospholipids are the most useful nuclei for NMR. For example, the relaxation time of water (hydrogen) in certain tumors is longer than normal [16]. Magnetoencephalography developed as a result of MRI and uses ultrasensitive devices called Superconducting Quantum Interference Devices (SQUIDS) to detect the magnetic flux of active neurons and convert it into electrical signals. Similarly, Electrical Impedance Imaging is based on the

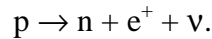
variation in electrical properties of tissues. The technique is useful mainly in the improvement of image contrast and resolution [17].

The first technique to be discovered for imaging the unseen used x-rays. Aside from the traditional application of x-rays, several new techniques have emerged recently. These include Digital Radiography, Digital Subtraction Angiography, used to image blood vessels, and Computer Tomography, made more versatile and useful by recent advances [17].

The technique most applicable to this project is Radioisotope Imaging. Radioactive isotopes can be used in the study of biological processes since their chemical properties do not differ from those of the corresponding stable element. The first study to use artificial radioisotopes was conducted in 1935, using radioactive phosphorous [18]. Currently many different isotopes are available for use in biological imaging. The oldest method and currently most used is Autoradiography. For this technique, the radioactively labeled compound is injected into several animals which are then sacrificed at different times after injection. Each animal is frozen and sliced into thin sections. Photographic plates are exposed to these slices and the images produced can be reconstructed to show the total distribution of radiation in the animal at the times chosen [19].

Newer techniques using radioisotopes are currently being developed that allow *in vivo* imaging. These include Single-Photon Computed Tomography (SPECT) and Positron Emission Tomography (PET), both of which produce three-dimensional images. SPECT recreates an image of the distribution of an injected radioisotope by rotating a photon detector around the animal [20]. PET works in a similar manner, except the radioisotope used decays by positron emission rather than photon emission. When the

nucleus contains too many protons for stability, a proton can convert into a neutron, emitting a positron (a positive electron) and a neutrino [21] . This process can be represented by the equation



When a positron encounters a free electron, which usually happens within 1 mm of emission, the two annihilate each other producing two photons ejected in opposite directions. In PET, the detectors are stationary but many are placed around the animal being imaged. When two photons are detected simultaneously 180° apart, their origin, and hence the position of the decay, can be deduced [22].

## B. Detectors

### *1. Scintillators*

Biomedical imaging relies on the detection of particles that give up some or all of their energy to a detector material. Most commonly used are electrons, x-rays, and gamma-rays. To detect high energy x-rays and gamma-rays, scintillators are used. Scintillators take advantage of materials that absorb certain forms of energy and re-emit that energy in the form of visible light, a property known as luminescence. When photons strike the scintillator material, they excite the atoms and molecules which then emit photons in the form of visible light when the atoms de-excite [23].

While several different kinds of scintillator materials are available and useful for detectors, the system at William and Mary uses an inorganic crystal. Inorganic crystal scintillators have the highest light output which makes them useful for low energy gamma-ray detection. Such scintillators rely on the properties of the electronic band

structure found in crystals. A gamma-ray entering an inorganic crystal will excite an electron and thus leave a free hole. These electrons are either free or are bound to the free hole they created to form an exciton. All three can move freely through the crystal. When a free hole encounters an impurity, it can ionize that atom [23]. The following de-excitation that occurs emits radiation in the form of visible light which is detectable by a photomultiplier tube.

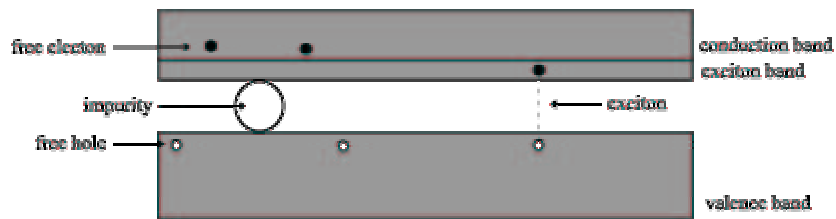


Figure 1. electronic band structure of inorganic crystals

## 2. Collimators

Collimators help reduce noise by absorbing photons that are most likely not coming from the source being imaged. There are two types of collimators that are useful for biological imaging: parallel-hole and pinhole. Parallel-hole collimators absorb photons that are not emitted from a direction nearly perpendicular to the scintillating crystal and are equally sensitive to all parts of the field of view [24]. Pinhole collimators have the best sensitivity and resolution for objects closest to the pinhole [25].

The ratio of imaging photons transmitted by a parallel-hole collimator to those produced by the source is called the geometric acceptance and is represented by the equation

$$1. \Omega = [Kd^2/a_c(d + t)]^2,$$

where  $K$  is a constant that depends on the shape of the holes and their distribution pattern,  $d$  is the width of the holes,  $t$  is the thickness of the septa, and  $a_e$  is the effective length of the holes. The effective length,  $a_e$ , depends on the total linear absorption coefficient of the collimator material,  $\mu$ , and is given by

$$2. \quad a_e = a - 2\mu^{-1}.$$

Their geometric resolution is given by

$$3. \quad R = d(a_e + b + c)/a_e$$

where  $b$  is the source-to-collimator distance and  $c$  is the collimator-to-scintillator distance [26].

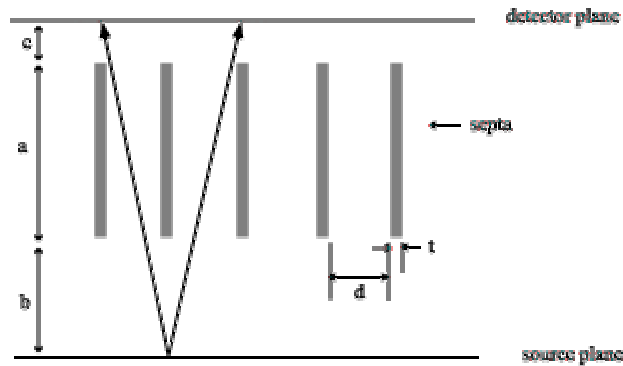


Figure 2. Parallel-hole collimator geometry

The geometric sensitivity of a pinhole collimator can be represented by the equation

$$4. \quad g = (d_e^2 \sin^3 \theta) / (16b^2),$$

where  $d_e$  is the effective diameter of the pinhole,  $\theta$  is the angle of the photon's path to the detector, and  $b$  is the distance from the source plane to the pinhole. The effective diameter is given by

$$5. d_e = [d(d + 2\mu^{-1} \tan(\alpha/2))]^{1/2},$$

where  $\mu$ , once again, is the linear attenuation coefficient and  $\alpha$  is the acceptance angle of the pinhole aperture [27]. Depending on the collimator-to-scintillator distance, the source being imaged can be magnified [28].

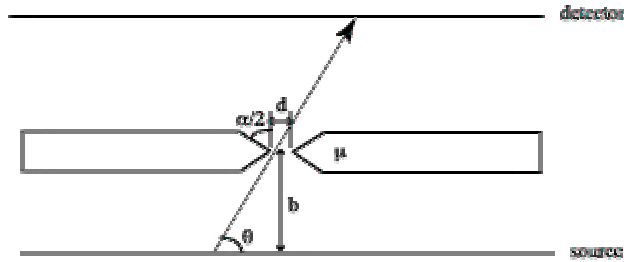


Figure 3. Pinhole collimator geometry

### 3. Photomultiplier Tubes

The faint light pulse emitted by a scintillator is converted and amplified by a photomultiplier tube into an electrical signal. Entering photons strike the photocathode, a semiconductor photosensitive material, and through the photoelectric effect electrons are liberated from the material. An electric potential guides and accelerates these photoelectrons through a series of dynodes. Each dynode consists of a conducting material covered by another material that releases three or four secondary electrons for every one that strikes it. The resulting multiplied cloud of secondary electrons eventually reaches the anode. At the anode, the electron cascade produces a current pulse which can then be amplified and eventually analyzed [29].

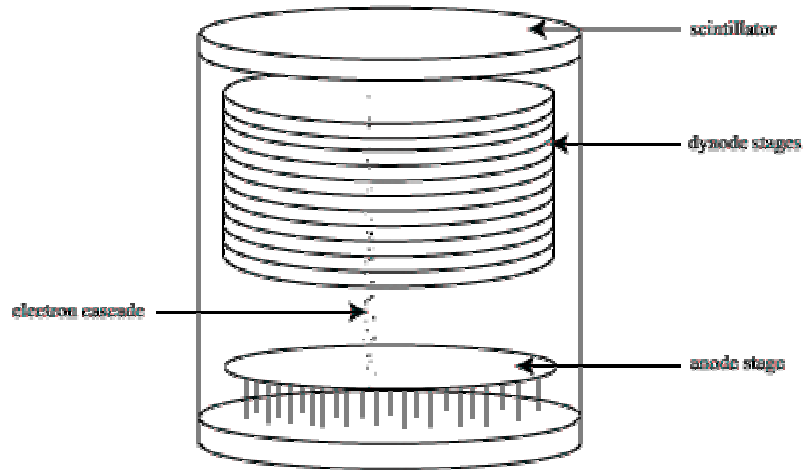
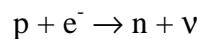


Figure 4. Position-sensitive photomultiplier tube

### C. Iodine-125

This project uses the radioisotope  $^{125}\text{I}$  as the label of interest. There are several advantages to  $^{125}\text{I}$  as compared with other available isotopes. For example, with a half-life of 60.2 days,  $^{125}\text{I}$  can be used at a facility that does not have access to the nuclear reactors required to produce the radioisotope. Another isotope of iodine commonly used for medical imaging,  $^{131}\text{I}$ , has a half-life of only 8 days, making it less suitable [30]. In addition, high-resolution imaging is more difficult with the higher energy emissions of  $^{131}\text{I}$  because of their increased penetration [31].

When the neutron to proton ratio in a nucleus is too low for stability, the nucleus will undergo radioactive decay to replace a proton with a neutron. Positron emission is one form of decay; electron capture is another and can be represented by the equation



An orbital electron is captured by the nucleus and combines with a proton to produce a neutron and a neutrino [32]. If the ground state spin of the daughter nucleus is different than that of the parent nucleus, the decay will most likely produce an excited state of the

daughter nucleus. The excited nucleus will subsequently emit a gamma ray in its de-excitation [33]. To produce  $^{125}\text{I}$ , xenon-124 is bombarded with neutrons from the fission of uranium-235. This produces unstable xenon-125 nuclei which then decay via electron capture into the radioactive daughter product iodine-125.

Iodine-125 decays via electron capture, producing the excited state of  $^{125}\text{Te}$ . In 93% of Tellurium's de-excitations, the excited nucleus will interact with one of the inner orbital electrons in a process called internal conversion. A virtual photon transfers all its energy to an electron, usually in the K shell, which is subsequently ejected from the atom. This leaves a vacancy in the orbital shell which is filled by another nearby electron. The energy difference between the orbital shells results either in the emission of characteristic x-rays, called the K-line, or is transferred to outer orbital electrons which are ejected as Auger electrons [33]. In  $^{125}\text{Te}$ , the characteristic x-rays have energies of 27-32 keV. In the remaining 7% of the de-excitations  $^{125}\text{Te}$  emits a 35 keV gamma-ray. Our imaging technique detects the 27-35 keV photons, which are produced at a rate of about 1.5 per  $^{125}\text{I}$  decay.

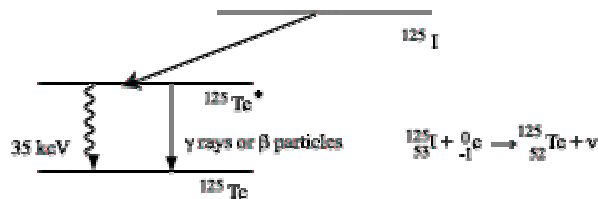


Figure 5. The decay of  $^{125}\text{I}$

## IV. DUAL-MODALITY

### A. Structural Information

The gamma detectors currently in use (see Section V. for system details) can achieve resolutions on the order of one to two millimeters. Two capillary tubes 1 mm in diameter separated by less than two millimeters can be resolved as two separate lines with a line of no activity between them. The tubes can be resolved as distinguishable but touching lines at smaller distances.

The mice being studied are, on average, seven centimeters in length. Thus, various organs are separated by only a few millimeters. The head region is an excellent example, since the thyroid, brain, and sub-maxillary glands are all contained within a region of approximately 1 cm. Since iodine is biologically active, if it should dissociate from the ligand of interest it can accumulate in the thyroid and salivary glands in its atomic form. While the gamma detectors can resolve separate spots for these regions, without accurate structural information it is impossible to tell exactly which organs those spots correspond to. The determination of the exact location of the radioactivity is essential to any study, not only to determine whether or not it is due to atomic iodine or the compound of interest, but also to determine the biological activity of the ligand.

An x-ray image that shows the bone structure as well as some of the major organs, and when co-registered with the gamma image can provide the necessary structural information to determine precise locations of radioactivity.

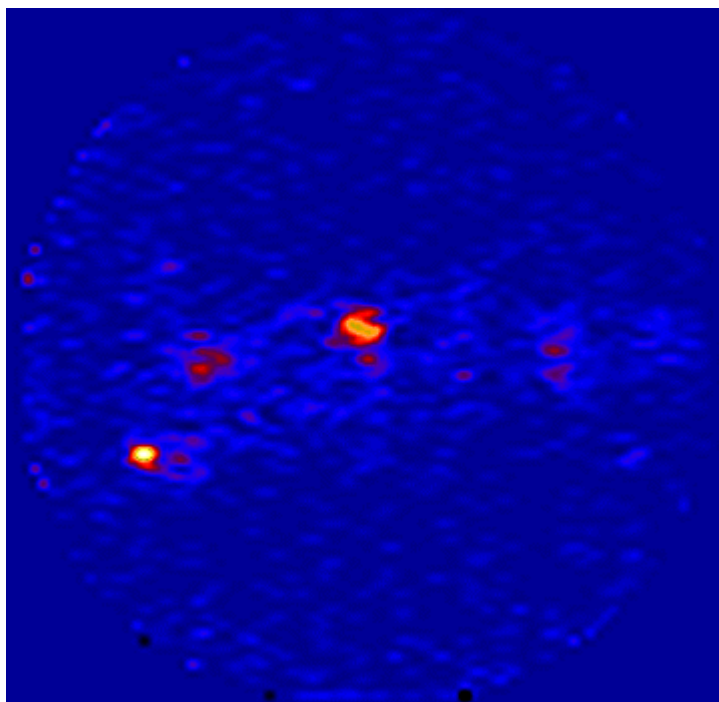


*Figure 6. A gamma image alone does not provide enough information for a biology researcher.*

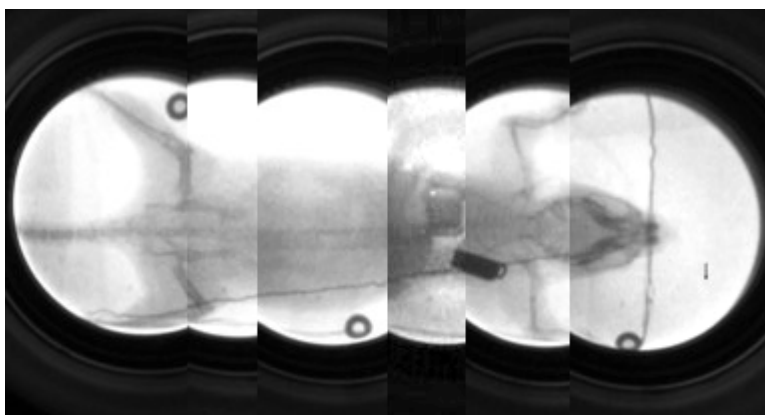


*Figure 7. An x-ray image provides the necessary structural information about the mouse.*

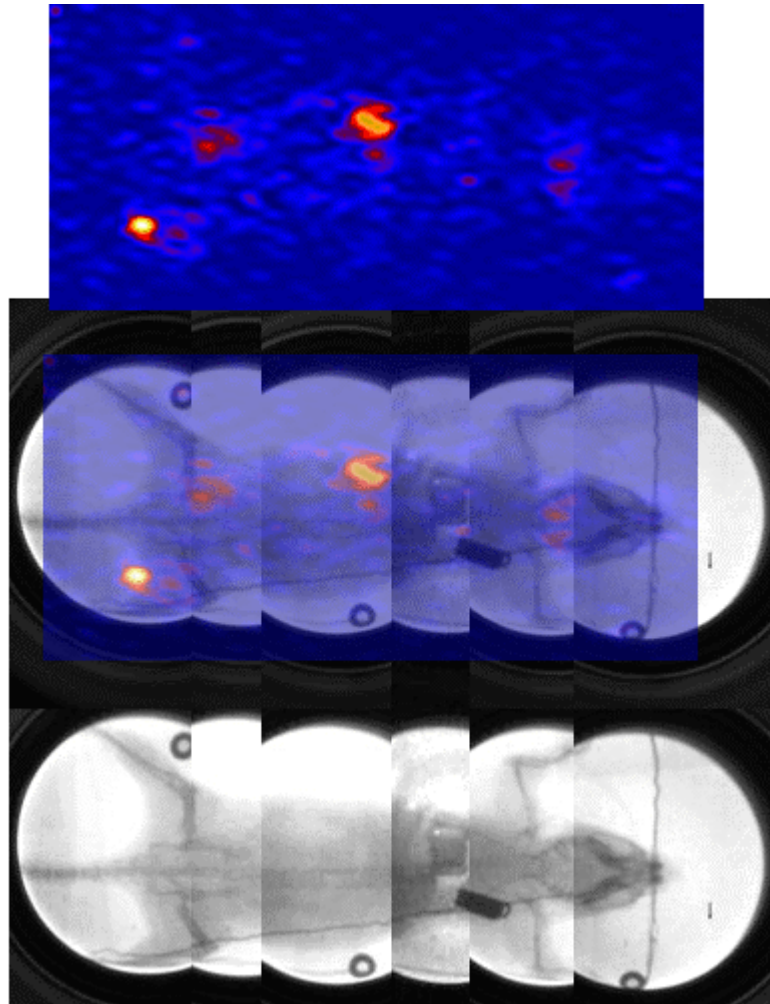


*Figure 8. The gamma and x-ray images can be co-registered to form a composite image with information from both.*

## B. Implementation

To gather useful x-ray images to provide accurate structural information for each mouse, a Lixi, Inc. fluoroscopic x-ray has been added. The Lixi has been mounted next to the gamma detectors so that the fluoroscopic screen is level with the face of detector A in its most common position. Parallel wooden rails run between the x-ray and the gamma detectors, and the face of detector B is placed as close to the bottom of these rails as possible. This allows for the best resolution achievable. The mouse is placed on a bed

made of balsa wood that is supported by these rails. Thus mouse bed can be moved between the gamma detectors and the x-ray machine, making it possible to bring the mouse from the x-ray to the gamma detector without changing its position on the bed.



*Figure 9. Lixi Fluoroscope with parallel wooden rails leading to the PSPMTs.*

Since the field of view of the Lixi fluoroscope is only 2 cm wide, a series of snapshots must be taken. Between each of these snapshots, the mouse bed is moved 1.5 cm along the rails. A ruler has been placed on the front rail to accurately measure this distance. Six images are usually taken to accommodate the entire animal. The images produced on the Lixi's fluoroscopic screen are viewed with a video camera. The camera is connected to a frame grabber which is interfaced with a Macintosh G3 computer. Using the photocapture software packaged with the frame-grabber, each image is taken and stored digitally on the computer. These frames can later be retrieved and reconstructed into one complete x-ray using Adobe Photoshop software. A thin diagonal wire has been placed in the mouse bed to aid in proper reconstruction of the x-ray image.

This counteracts any vertical offset that might occur between frames. The frames are aligned horizontally based on the animal's structure.

Recently a digital camera was purchased to replace the analog camera that has been in use for the past year. Instead of converting an analog video stream to a digital image, the new camera will send digital images directly to the computer via a standard USB connection. This will reduce degradative effects and loss of resolution. Reconstruction will also be made easier since structures can be seen more clearly. The new camera will improve the quality of the x-ray images stored and hence their usefulness as structural references.

### C. Co-registration

In order for the structural information gathered with the x-ray to be useful, a means of ensuring accurate co-registration must be used. For this reason, small metal washers have been filled with plaster-of-paris which has then been soaked with Na[<sup>125</sup>I]. These produce a small dark circle on the x-ray image and a small bright spot on the gamma image. Washers have been placed in three of the four corners around the outside of the animal. The fourth corner corresponds to the injection site for the tagged ligand. This produces a large bright spot which would overlap that of the washer. Not only would it make the fourth washer superfluous, but the corresponding data for the injection site would be corrupted by the hot washer.

The first washers used were slightly larger than those currently on the mouse bed and produced a spot that was rather large. We have thus chosen washers with 2 mm central holes to allow co-registration of images to within about 1 mm precision. The

washers are occasionally resoaked with Na[<sup>125</sup>I] when the isotope has decayed beyond the point of producing useful spots.

Currently, co-registration is done manually using Adobe Photoshop software. The gamma image is rotated so that the line between the lower two washers corresponds to the same line on the reconstructed x-ray. This rotation is usually 3-6 degrees. While attempts have been made to maintain the exact orientation of the detectors when they are removed from their brackets, this has not been possible, creating the differences in rotation needed. Once the gamma image is oriented correctly, it is layered with the x-ray image with 50% opacity, allowing the corresponding bone structure to be seen. The bright spots of the washers are then aligned in the center of the dark rings.

## V. SYSTEM DETAILS

### A. Gamma Detectors

Two Hamamatsu R3292 PSPMTs are currently employed in the system. These detectors have a diameter of 125 mm. The photocathode material is bialkali, which is frequently used in conjunction with scintillators, whose emission spectra match its spectral response. There are twelve coarse mesh dynode stages which have a high pulse linearity and allow position detection [34]. The anode stage of the R3292 consists of  $28(X)+28(Y)$  wires which we have paired into  $14(X)+14(Y)$  groups to reduce the number of electronic channels needed. The two PSPMTs being used, referred to here as A and B, have been placed  $180^\circ$  apart facing each other. Approximately 5 cm has been left between the two detectors for the rails, mouse bed, and mouse. This leaves enough room to monitor the mouse's breathing.

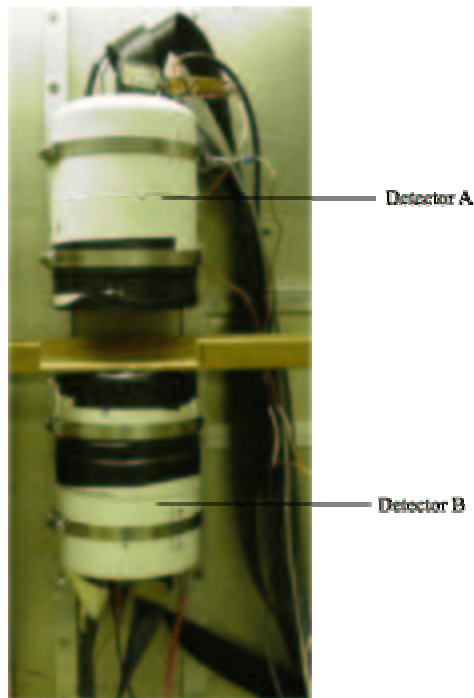


*Figure 10. PSPMT setup: detectors A and B have different collimators to provide different resolutions and sensitivities. The mouse is placed between the detectors for imaging.*

Coupled to each of the PSPMTs is a sodium doped cesium iodide [CsI(Na)] scintillating crystal array. To improve spatial resolution and reduce image distortion, these scintillators have been pixilated, cut into an array of small crystal elements. Scintillating crystal pixels direct photons onto the photocathode with less light spread that would occur with a single planar scintillator [35]. Pixilated scintillators also provide a relatively large field of view coupled with high detector efficiency [36].

In front of each scintillator is a collimator. For most of the studies, two copper-beryllium (CuBe) parallel-hole collimators have been used. These collimators are constructed by the Thermo Electron Corporation from 40 layers of CuBe laminates that have been glued together. This results in a total thickness of 0.5 cm. The collimator used with detector B has square holes 0.2 mm wide separated by septa 0.05 mm thick. Detector A has had a collimator with holes 0.75 mm wide separated by 0.16 mm septa. With these collimators, detector A provides higher sensitivity but lower resolution, while detector B provides lower sensitivity with higher resolution. We have been able to resolve a pair of capillary phantoms filled with Na[<sup>125</sup>I] using detector B with the tubes placed on its face a distance of 2 mm apart.

Recently experimentation has begun with pinhole collimators on detector A instead of the low-resolution parallel hole collimator. These could prove useful for imaging smaller mice organs like the brain and pancreas. The pinhole collimators are all made out of brass and have been constructed for either the 125 mm PSPMTs currently in use or the 25 mm PSPMTs which are to be incorporated. 125 mm collimators have been constructed with 1 mm and 2mm pinholes; 25 mm collimators have been constructed

with 1mm, 2mm, and 3mm pinholes. The best results so far have come from the 125 mm collimator with a 1 mm aperture with a pinhole-to-scintillator spacing of 2 inches.

## B. Electronics

Each signal from the 28 paired anode wires is amplified and delayed before being sent to 28 individual ADC (Analog-to-Digital Converter) channels. Each standard ADC module (LeCroix) in a Sparrow, Inc. CAMAC Crate is sent either the 14(X) or 14(Y) channels from a detector. Thus, for two detectors, there are four ADC modules. The CAMAC system has been designed to use a crate with variable plug-in modules. Each module is coupled via an 86 pin connector to a series of parallel wires called the dataway. Communication between modules is overseen by a crate controller which is also interfaced to the computer [37].

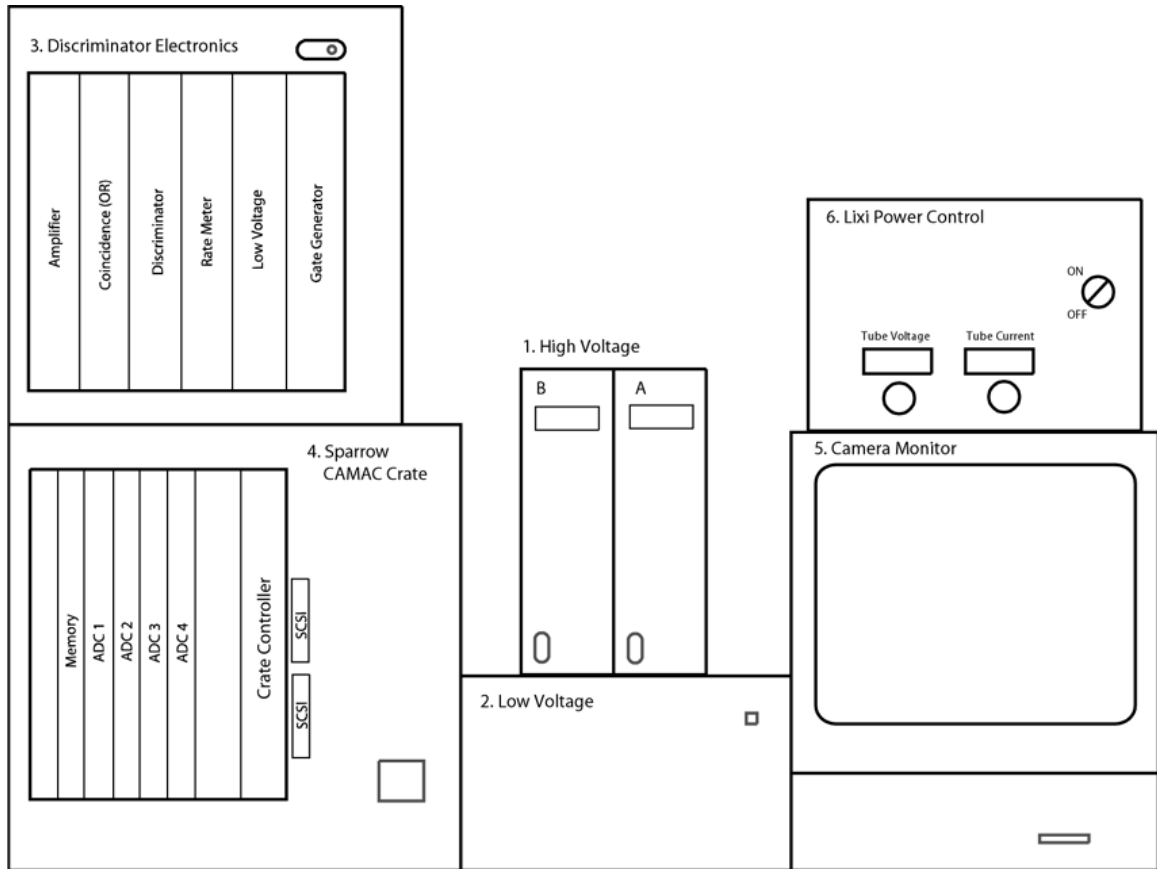


Figure 11. Electronics: dynode signals are sent to discriminator electronics and analog signals from the PSPMTs' anodes are sent to the CAMAC Crate. The high voltage provides the 1000 V potential to accelerate electrons through the dynode stages of the PSPMTs.

Two dynode signals, one from detector A and another from detector B, are sent to the discriminator electronics. These electronics are necessary since the system will be faced with signals from competing events and noise. The discriminator limits the generation of output signal to pulses that exceed an empirically determined threshold level. The signals are also sent through an exclusive OR gate so that only one detector triggers an output signal at a time [37]. The signals are sent from the Crate to a Macintosh G3 computer via a SCSI connection.

### C. X-ray

The system incorporates the Lixi LF-85-5 3-OS Real Time Pulse X-ray System. Short pulses of x-rays are generated and detected by a scintillator screen. This fluoroscopic screen is viewed with an American Dynamics CCD Camera (AD650). The analog camera is interfaced to the computer with a GlobalVillage photocapture device.

### D. Mouse Bed

A specialized bed to hold the mouse during imaging has been constructed to address concerns encountered by imaging a live mouse for periods of time on the order of an hour. The bed is made of two layers of balsa wood with two pieces of foam padding. This padding supports the mouse and helps prevent its tissue from sagging over time. Such sagging can change the tissue's position and thus change the image distribution. The mouse's position would also no longer correspond to that in the x-ray image.

Secondly, three thin nichrome wires have been run between the two layers of balsa and connected to a power source. These are supplied with approximately 5 W and provide a source of mild heat. When the mouse is anaesthetized, its metabolism slows and therefore its body temperature drops. By heating the mouse, its metabolism can be maintained at a more normal level. This maintenance is important since the biodistribution of a ligand depends partly on the mouse's metabolic rate.

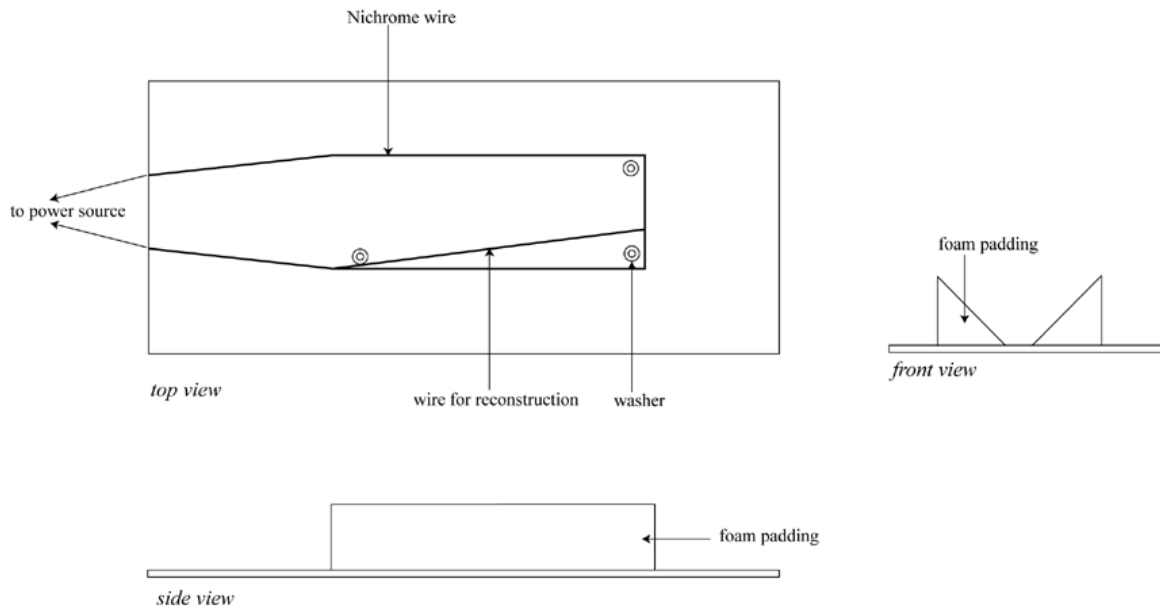


Figure 12. Mouse bed equipped to provide for the needs of an anesthetized mouse: support and heat.

The metal washers used for co-registration are placed underneath the foam padding. Also beneath the padding, yet on top on the balsa wood one can include a thin diagonal wire to aid x-ray reconstruction. The nichrome heater wires are generally out of the field of view of the x-ray.

## VI. DATA ANALYSIS

### A. Time Cuts

Data that are sent from the CAMAC Crate are stored event by event by a program written using Kmax (Sparrow, Inc.). This software is designed to allow instrument control and data management specific to the system setup. The data acquisition program stores the data as event files which map the raw images to corrected ones based on the response of the pixilated crystal scintillator array. This corrects for the PSPMTs inherent non-uniformity in its spatial response. These files may subsequently be analyzed using other programs. For shorter runs, data can be taken and stored simply as histograms, which are still corrected using the Crystal Lookup Tables. This method is useful for SPECT runs.

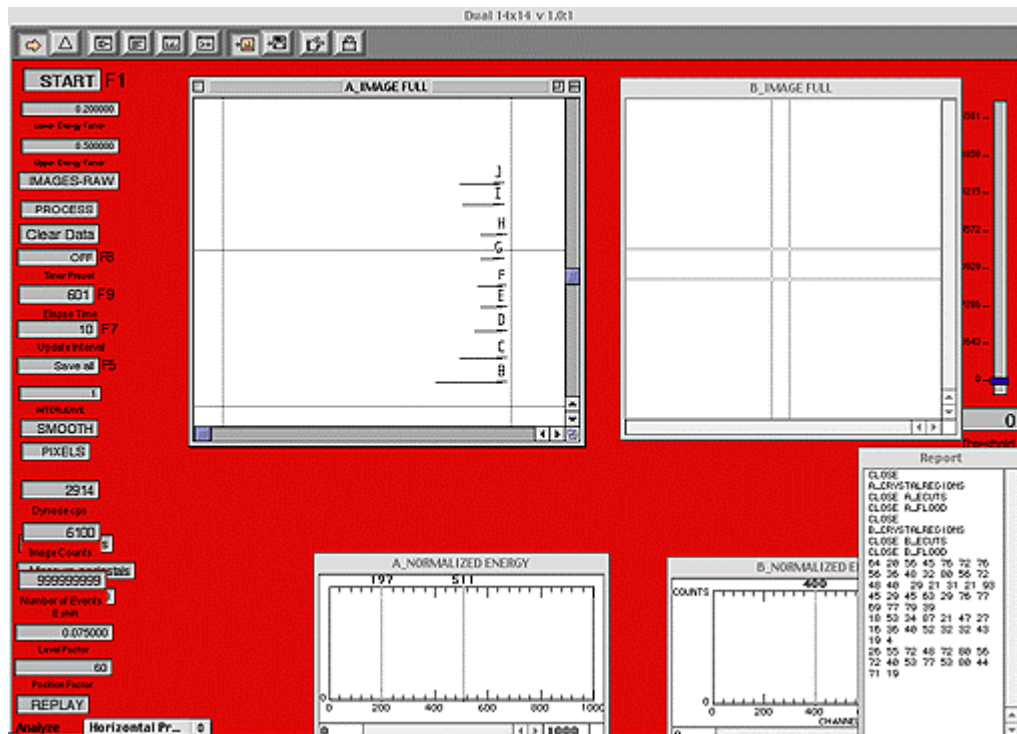
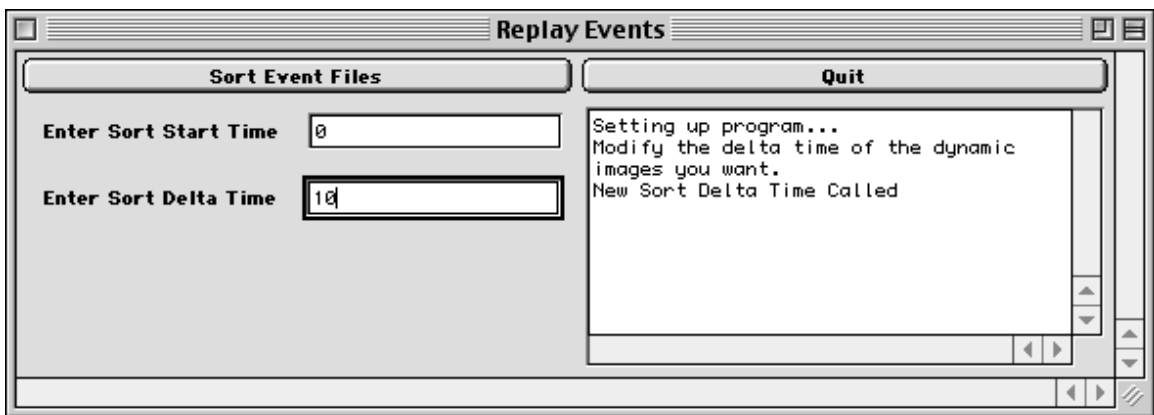


Figure 13. Data Acquisition user interface: stores data event by event in real time.

Once an entire run has been imaged, a data analysis program written in IDL (Interactive Data Language, Research Systems, Inc.) allows the user to divide the data into useful segments of time. The program sorts through data beginning at a specified start time and reconstructs it into consecutive data sets of a specified time interval. Currently, the most useful time allotment is ten minutes, giving 5 or 6 images for a one hour run.



*Figure 14. Time Cuts program user interface: sorts event files into useful histograms of user-determined start and delta time.*

## B. Regions of Interest

Once the data have been stored as time cuts, they can be analyzed using another program written in IDL. The analysis program takes a data histogram and displays it using the appropriate flood correction. Such a correction is necessary because the sensitivity of the PSPMT is also non-uniform. A flood image is obtained using a uniform radioactive liquid source placed approximately 10 cm from the detector. When a histogram is displayed in the IDL program, each pixel is corrected in comparison with others based on the flood image. The flood correction is performed by determining the average value of all non-zero pixels then making a correction image by multiplying the

flood image pixels by the inverse of this average. Each pixel of the histogram loaded is multiplied by the corresponding pixel of the correction image.

The data analysis program has a feature called Region of Interest (ROI). A square ROI of user-determined size can be placed anywhere on a given displayed histogram. The program will then compute the number of counts within that region in that image. More importantly, the Analyze ROI function produces a graph of the counts in that region for the entire length of the run. This feature has recently been improved to display the data table used to make this plot in a report window. This process can be repeated as many times as desired, allowing extreme flexibility in analysis. In addition, the graphs provide a more accurate means of comparing mice since they do not rely on human visual interpretation of colors on an image.

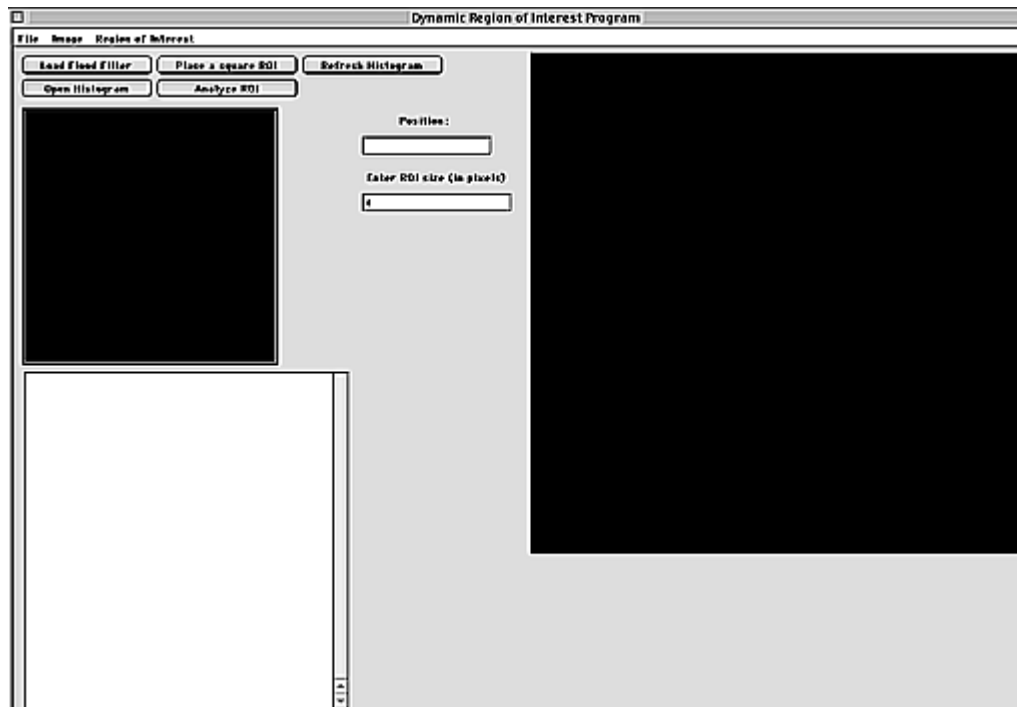


Figure 15. Data Analysis user interface: displays an image of a histogram. The Region of Interest, with user-determined size and position, can be analyzed to provide a plot for the region of the entire run.

### C. SPECT

Single-Photon Computed Tomography, known as SPECT, allows a series of several planar images taken at regular angular intervals to be reconstructed into a three-dimensional image. Such a technique is particularly useful when activity may accumulate in small overlapping organs. A planar view might merely produce one indistinguishable spot. With a three-dimensional image, such organs can be differentiated. Such is the case with the current study. [<sup>125</sup>I]-Insulin can accumulate in the pancreas, stomach, and/or liver of a mouse. The organs overlap in the mouse's abdomen when viewed from the top or bottom, as occurs with the present detector setup. However, they can be distinguished when viewed from the side. Other organs can overlap when viewed from the side, but not from either the top or bottom. Thus it is necessary to acquire information about views in all three dimensions.

Preliminary work has been done to incorporate SPECT into the system at William and Mary. This work is based on a tomography algorithm called One Step Late written by Peter Green and translated into IDL by Dr. Steve Meikle of the Department of Radiology at the Royal Prince Alfred Hospital in Sydney Australia. Currently images are acquired by rotating a phantom 360° in 3° increments. Since each view must be imaged for at least three minutes to acquire sufficient statistics, the current arrangement is not practical for time-dependent studies that involve the metabolism of a substance [38].

## VII. DIABETES STUDIES

### A. Procedure

The first step in imaging *in vivo* is to anesthetize the mouse. Previously we had been using 4% chloral hydrate. Recently, however, we have switched to dilute pentobarbital which maintains a suitable level of anesthesia more evenly for the necessary duration than the previously used chloral hydrate. The anesthetic is administered through an intraperitoneal injection of 40 mg/kg body weight. An additional injection can be given to maintain stage IV surgical anesthesia. Once the mouse has been sufficiently anaesthetized, the mouse is placed on the heated mouse bed and the tagged insulin is injected intramuscularly into the right femoral bicep. Suitable results have been obtained using only 1-2  $\mu\text{Ci}$  of activity, which corresponds to 50-100  $\mu\text{L}$  of receptor grade [ $^{125}\text{I}$ ]-Insulin.

Next, the series of x-ray shots is taken. The mouse is moved 1.5 cm between each shot to allow for the most efficient reconstruction. The x-ray is turned on only briefly for each view to minimize exposure to both the mouse, since it is being imaged *in vivo*, as well as the researchers.

Once the x-ray series has been completed, the mouse bed is brought to gamma detectors. The bed is placed so that the entire animal and the loaded washers are in the field of view of detector B. Since detector A is coupled with a pinhole collimator, its field of view is much smaller. Data are taken until one hour after injection of the radiopharmaceutical, when the mouse is returned to its cage to recover.

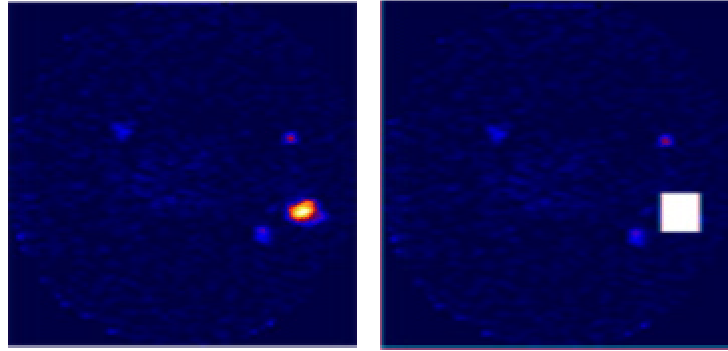
The mouse is re-anaesthetized later with 20-30 mg/kg dilute pentobarbital. It is placed once again on the mouse bed and x-rayed prior to starting data acquisition at three hours post-injection. Four hours after injection, imaging is stopped and the mouse is once again returned to its cage.

## B. Current Results

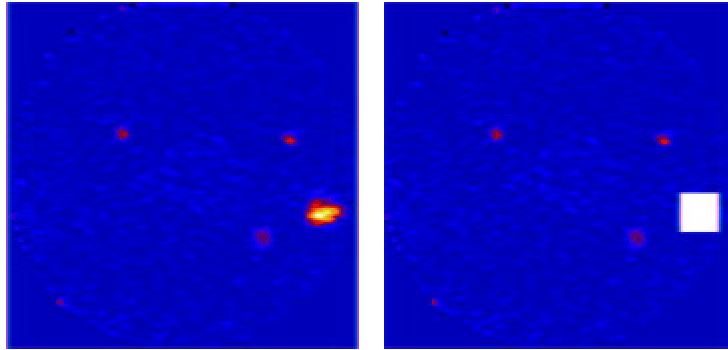
From a biology standpoint, few concrete statements can currently be made. Interesting results have been obtained however. Image analysis shows that SZT-treated mice have more counts in a given location of the body at a given time after injection than do the control mice. This takes into account relatively little variation in the counts shown in the injection sites ten minutes post-injection. The following images are from mice 19, 20 and 21 in order. Mice 19 and 21 were SZT-treated and mouse 20 was a control. While the counts in all three images are nearly the same at time 0 (10 min post-injection), the counts in the two SZT-treated animals at time 40 are both approximately twice that of the control at time 40.

In the third hour after injection, this observation is confirmed. A comparison between the pancreatic region of mouse 21 (SZT-treated) and mouse 20 (control) shows consistently more counts in mouse 21. This trend was observable in other mice and in other regions of the body.

Counts in ROI are 731.804		
time	counts	sigma
0	731.804	27.0519
10	667.163	25.8295
20	586.273	24.2131
30	488.916	22.1114
40	508.520	22.5504



Counts in ROI are 800.429		
time	counts	sigma
0	800.429	28.2919
10	337.058	18.3591
20	272.120	16.4961
30	220.032	14.8335
40	253.849	15.9327



Counts in ROI are 923.626		
time	counts	sigma
0	923.626	30.3912
10	668.342	25.8523
20	589.976	24.2894
30	494.101	22.2284
40	507.631	22.5307

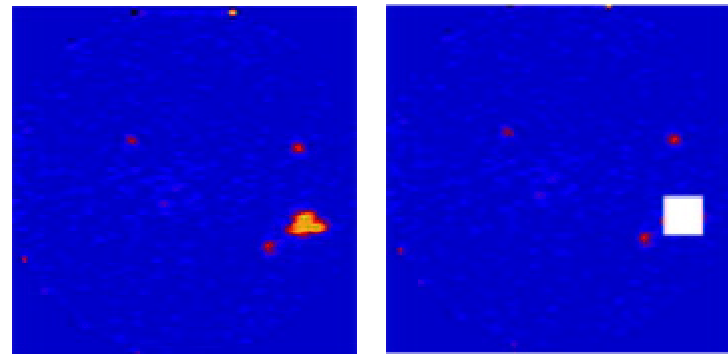
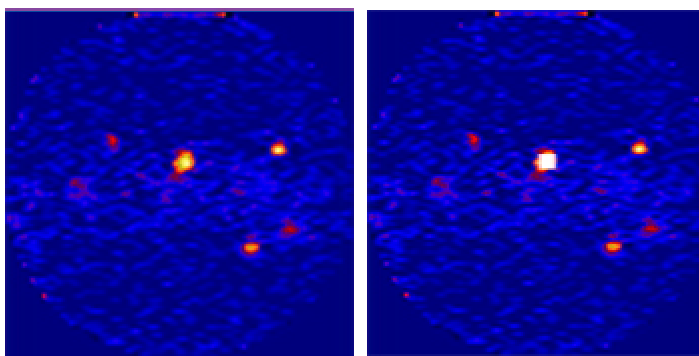
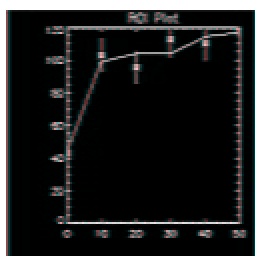
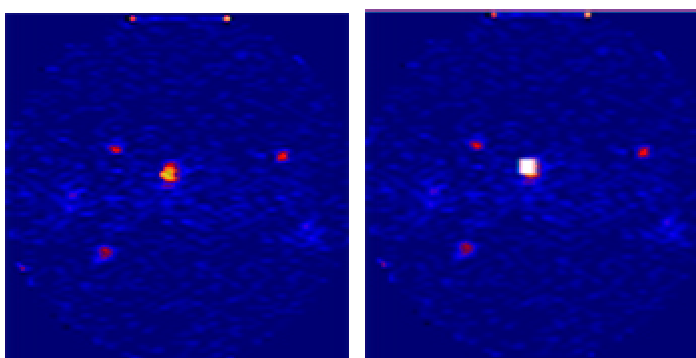
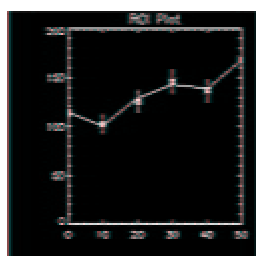


Figure 16. Comparison of injection sites: SZT-treated mice have consistently higher counts than control mice when starting with comparable rates.

**Mouse 20: Control**



**Mouse 21: SZT treated**



*Figure 17. SZT vs. control mouse three hours post-injection: the pancreatic region in the SZT-treated mouse shows higher counts than the control mouse. The findings were confirmed by RN-ase Protection Assay for insulin receptor mRNA.*

The detection system was confirmed using a Ludlum scintillation probe to count the radiation in various organs. These counts roughly corresponded to the ratio of counts seen in data analysis. In addition, the same trend comparing SZT-treated and control mice was seen in that the SZT-treated mice consistently had organs with higher count rates.

An RN-ase Protection Assay was also run on the organs of mice 14 and 15, which showed the same results as mice 19, 20, and 21, to determine the expression of insulin receptors. It was determined that the levels of mRNA for the insulin receptor gene were correspondingly higher in the SZT-treated animals than the control animals. This would appear to corroborate the findings based on the detector system and an additional

measure of organ count rates. This can tentatively be assumed to show more binding of radioactivity in areas and in animals with higher insulin receptor levels.

Currently the biggest disadvantage of the detector system involves areas of low count rate. While areas with high count rates show plots with stable slopes, areas with low count rates do not. At this point, it is not yet determined whether this is due merely to noise or some other factor.

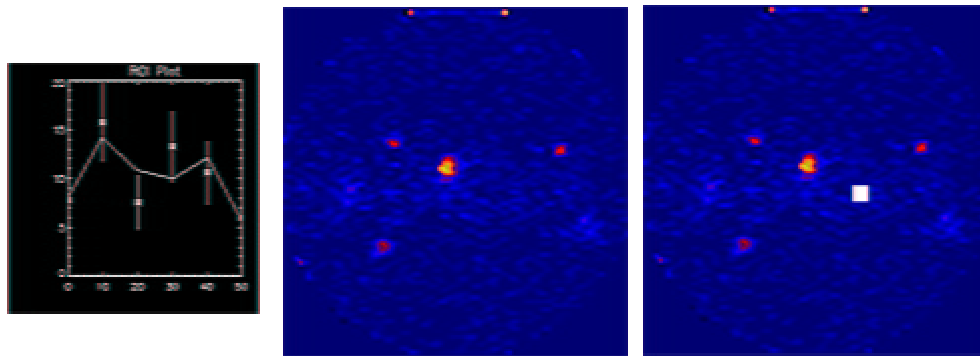


Figure 18. Low count rate regions do not have enough statistics to provide accurate graphs.

For one run, mouse 17, there was a much lower dose of tagged insulin, so the images for detector B were quite poor. The images for detector A, with the pinhole collimator, showed promise in that there was a noticeable spot that could be resolved into what is most likely two different organs.

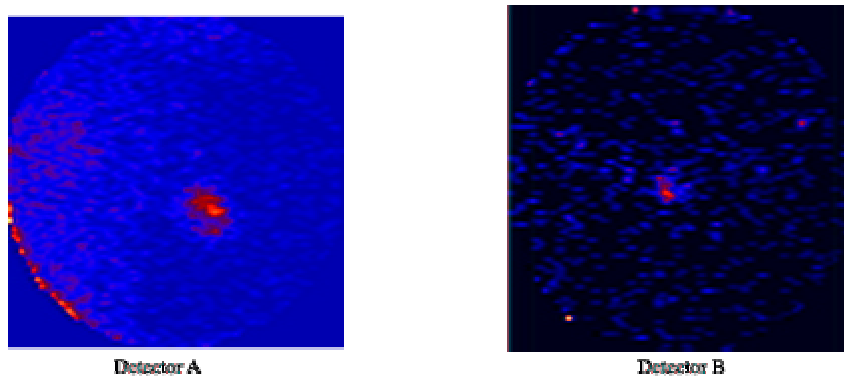
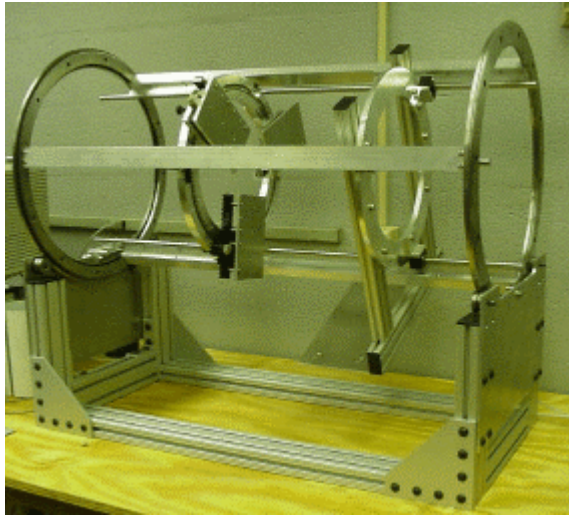


Figure 19. Pinhole collimated images can provide a magnified view of the pancreatic region in a mouse compared with parallel-hole collimated images.

## VIII. FUTURE IMPROVEMENTS

### A. Rotating Gantry

A rotating gantry for the detector system has been designed by Randy Wojick of Jefferson Lab and constructed by William and Mary's physics machine shop. This gantry can support many combinations of PSPMTs that would be used at William and Mary. The Lixi x-ray can also be mounted on the same gantry. This gantry will allow for a more compact and versatile system.



*Figure 20. Rotating gantry with mounts for the Lixi fluoroscope and a combination of PSPMTs.*

The gantry can rotate to provide SPECT support. To minimize the time needed to complete  $360^\circ$  of imaging, three PSPMTs can be mounted at  $120^\circ$  intervals. This will minimize the change in biodistribution between the first and last intervals imaged. An NF90 series Stepping Motor Controller (Velmex, Inc.) rotates the gantry to the desired angle. This will also help reduce the total time for a SPECT run, since an operator does not have to constantly move between computer and gantry.

Another stepper motor will control the horizontal movement of the mouse bed. One advantage of a stepper motor controlled system is higher accuracy when moving the bed between x-ray shots. In addition, the risk of rotating the bed, as exists with the current rail system, will be minimized. Further, as in SPECT runs, the ability to control movement from the computer will reduce necessary imaging time and exposure to x-rays.

#### B. M-64s

In contrast to the current Hamamatsu R3292-02s, which have a diameter of 125 mm, smaller 25 mm square R5900-M-64 PSPMTs will be incorporated into the system. These have several advantages over the larger tubes. First, they can be placed closer to the animal, allowing for higher resolution. They also allow for a greater specificity in imaging. For example, one can be placed directly next to the pancreatic region and exclude any counts that accumulate in the thyroid region. These detectors should also be extremely useful for research planned by Prof. Margaret Saha of the William and Mary Biology Department to study aging in the mouse brain. These detectors are ideal for SPECT imaging and the gantry has been designed to hold three M-64s at 120° intervals.

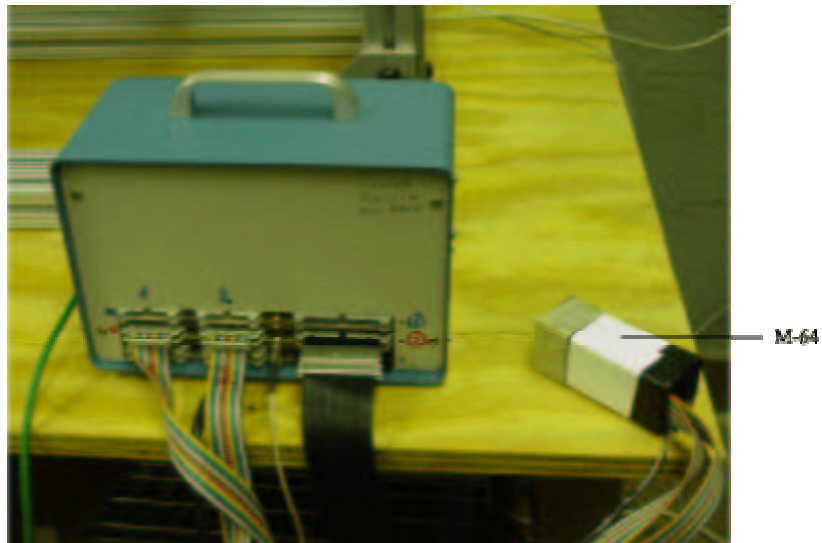


*Figure 21. M-64 PSPMT*

The M-64, like the R3292, has a bialkali photocathode. The dynode stages are of the metal channel type. These are an array of small, focused, linear dynodes that have a fast time response and allow position detection [39]. As opposed to the crossed wires of the R3292, the M-64 has an 8x8 multianode stage, whose 64 pads produce the electronic signals.

### C. Software

Currently both the x-ray reconstruction and image co-registration are done by hand. Both these processes would benefit from the development of an algorithm to do so digitally. A transformation to map one image to another with respect to intensity and/or structural information, must be found [40]. In our case, the transformation must match the center of the metal washers with the center of the hot spots they produce. Some current methods include Computer Vision and Pattern Recognition, which involves object recognition and shape reconstruction, Medical Image Analysis, and Remotely Sensed Data Processing [40]. One system at the University of Virginia uses a co-registration routine based on a linear array of  $^{99}\text{mTc}$ -filled wells [41].

### D. Statistics

The most significant problem with the system is the poor statistics obtained in most regions of the mouse's body. Currently, these regions produce unacceptable graphs. One way to increase counts would be to increase the amount of ligand injected into a mouse. There are, however, several biological considerations that put a limit on the amount injected. The first is the dose of radiation given to an animal. If the system

images animals *in vivo* to avoid sacrificing them, it would be counter-productive to kill the mouse with radiation poisoning. In addition, too high a dose of insulin, or any other compound, would have negative effects. Excessive doses of insulin can lead to diabetic shock caused by severe hypoglycemia. Flooding the system with insulin would also affect its biodistribution. If insulin receptors are up-regulated by its absence, as our preliminary results show, an overdose of insulin would consequently down-regulate the receptors and negate the effect of the SZT-treatment.

It is currently hoped that the M-64 PSPMTs will provide a solution to the problem of statistics. By placing the detectors closer to the animal, they will detect more counts without any of the adverse effects of increasing the dose. A count rate twice as high as the current rate might provide reasonable results.

## IX. CONCLUSIONS

The high resolution detector system being developed at William and Mary has the potential to be extremely useful in both clinical and research settings. It accommodates many of the new demands being placed on imaging technology. These include higher resolution and better accuracy, as well as *in vivo* techniques which are important for more humane animal testing. The system has recently been greatly improved by the addition of a second imaging modality. X-ray images provide vital structural information for the mice being imaged using  $^{125}\text{I}$ -tagged ligands.

Recent studies have shown the utility of the system and promise interesting results for further research. Future improvements are planned that will enhance the utility and benefits of the present system. The most significant of these would be an increase of statistics without harmful side effects of an increased dose. Additionally, the techniques used and problems solved can be applied toward imaging systems suitable for larger animals and humans.

## APPENDIX: INSTRUCTION MANUAL

### A. Data Acquisition

#### 1. Turn Equipment On

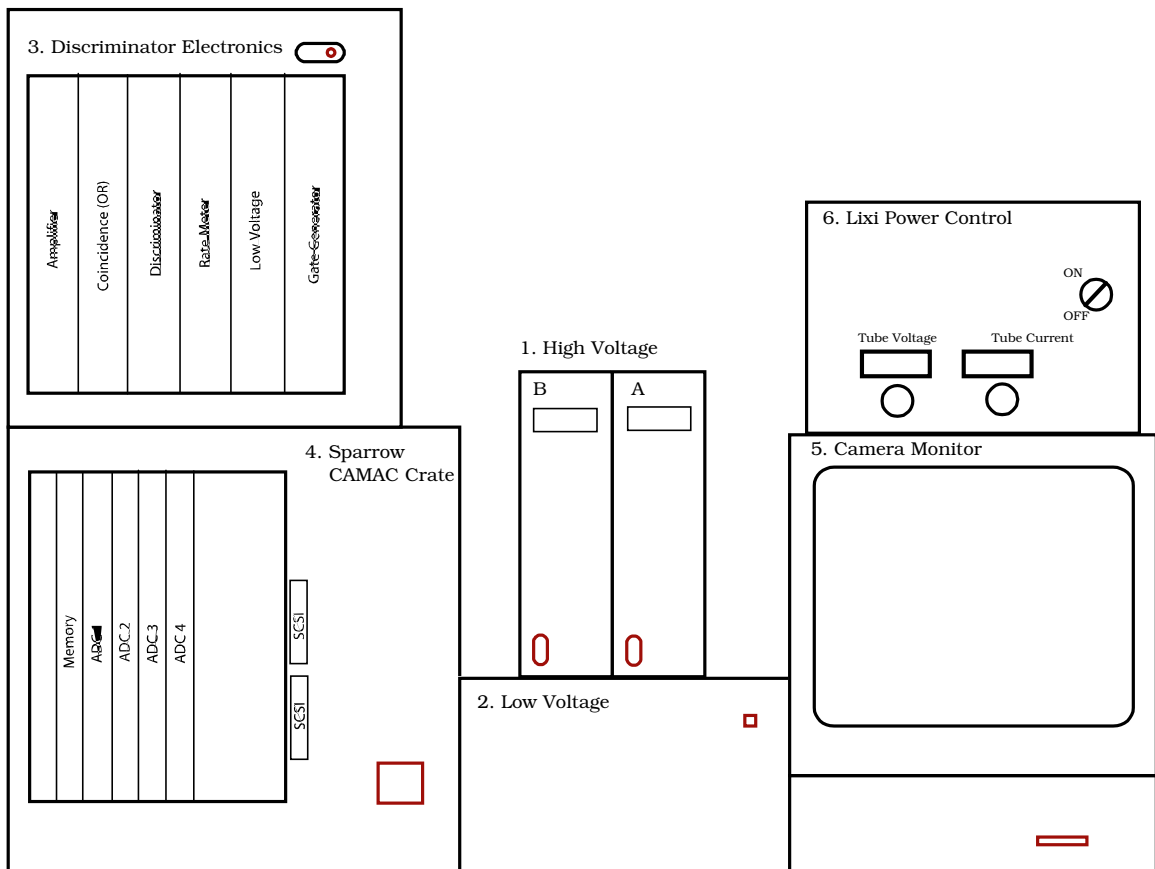
Make sure the computer is off. If it is on, shut it down.

To shut down the computer:

- Go to the top menu, click **Special**.
- Choose **Shut Down**.

Turn on the hardware in the following order:

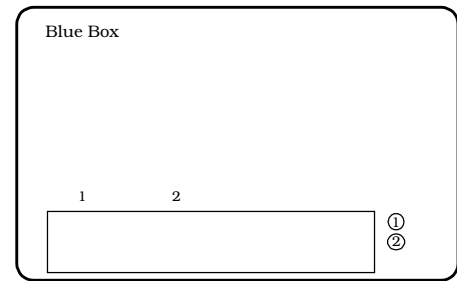
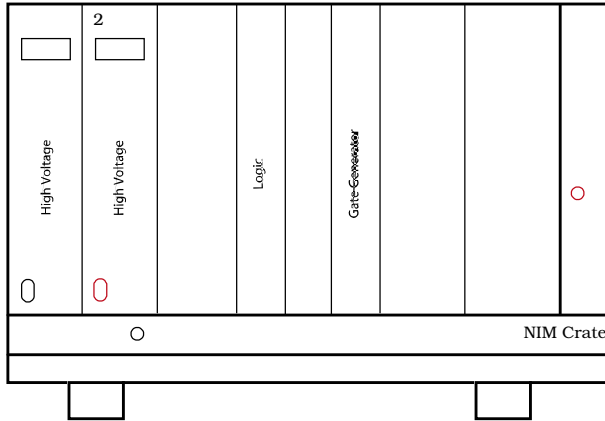
High Voltage  
Low Voltage  
Discriminator Electronics  
Sparrow Crate  
Camera Monitor  
Lixi Power Control



The power switches are marked in red. The Lixi Control's power switch is in the back on the right hand side.

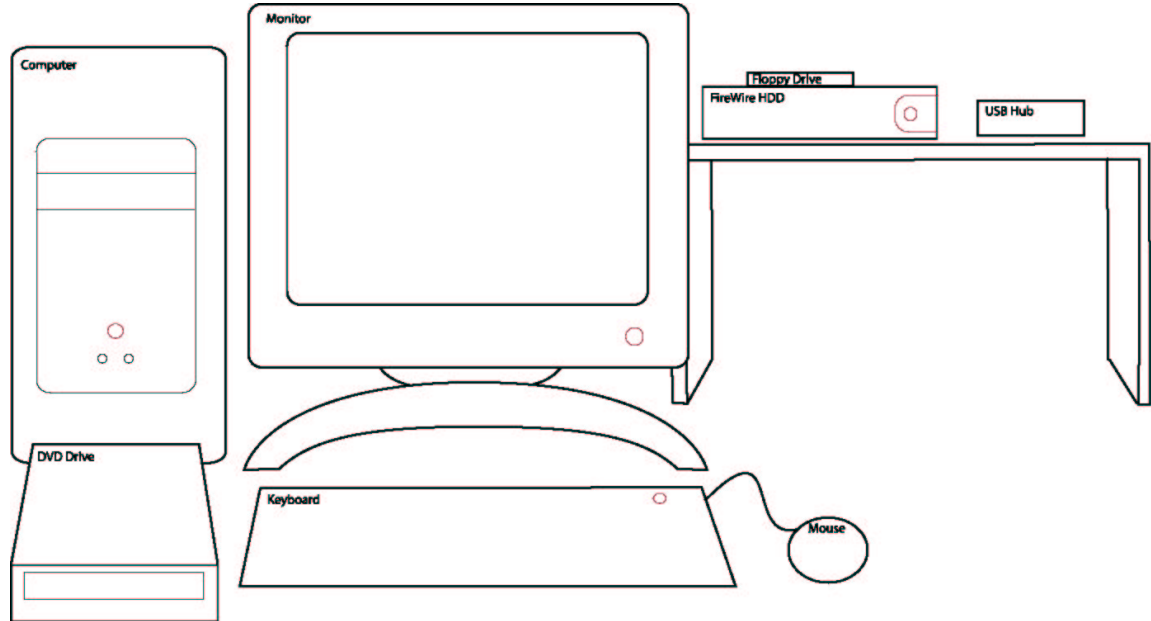
Turn on the 1" hardware in the following order:

- High Voltage
- NIM Crate
- Blue Box



Make sure all the computer components are on. The power switches are marked in red on the diagram below. The DVD Drive's switch is in the back on the left hand side.

Turn on the G3 by pushing the  button on the keyboard.



### Switching to 1" Detector

Make sure 1" equipment is turned on. You do not need to shut down the computer in order to switch to the 1" detector.

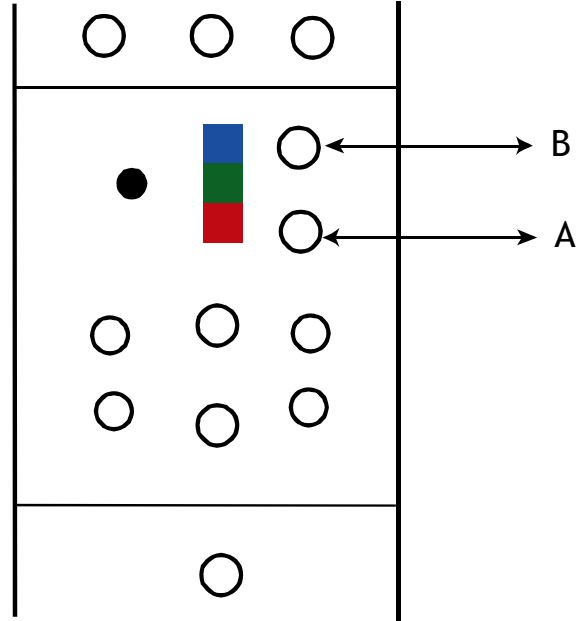
Place detector in desired position by mouse.

On the Coincidence module of the Discriminator Electronics:

- By the green label, remove the cable for either A (red) or B (blue), whichever 5" detector you do not wish to use.
- Plug the green cable into the open connector.
- Mark the green cable with the clothespin that matches the cable removed.

On the ADCs:

- Remove B's cables (blue) from ADC 3 and 4.
- Plug 1" cable (green) into ADC 4. All cables' tape should be facing to the right.
- Plug cables from either A (red) or B (blue) into ADC 1 and 2 with the X cable in ADC 1 and the Y cable in ADC 2.



Make sure to switch Data Acquisition program before taking data.

### Restoring A+B System

On Coincidence Module: Replace green cable with cable from whichever 5" detector was not used. This will be marked by the clothespin on the green cable.

On ADCs:

- Unplug 1" cable (green) from ADC 4.
- Plug A's X cable (red) into ADC 1 and A's Y cable (red) into ADC 2.
- Plug B's X cable (blue) into ADC 3 and B's Y cable (blue) into ADC 4.

Make sure to switch Data Acquisition program before taking data again.

## 2. Take an x-ray

Warm up the Lixi:

(note: make sure the mouse is outside the hood during this process)

- Set the **Tube Voltage** and **Tube Current** dials to 0.
- Turn key from **OFF** to **ON**.
- Increase the **Tube Voltage** and **Tube Current** dials in the following order, waiting one minute between each change.

<u>Voltage</u>	<u>Current</u>
10 kV	10 $\mu$ A
20 kV	10 $\mu$ A
30 kV	30 $\mu$ A
30 kV	60 $\mu$ A

Once the Lixi has been warmed up, turn the key to the **OFF** position.

Place the mouse bed on the rails with the marker at 0 cm.

Start the photo capture software:

- Double click on the **Global Village VideoImpression** icon.
- Click on the top left icon in the program window that looks like a movie reel with blank paper behind it. If you hold the mouse over the icon for a few seconds, it will say **New**.
- Click on the video camera icon.

Take pictures:

- Turn the key on the power control to the **ON** position.
- Click **Capture Photo** in the Global Village software.
- Turn key to **OFF**.
- Slide mouse bed 1.5 cm.
- Repeat until entire mouse has been x-rayed (usually at 7.5 cm).

Turn off the Lixi:

- Turn **Tube Voltage** and **Tube Current** dials to 0.
- Turn off power through rear switch.

### 3. Take Data (Event Files)

Create mouse's directory:

- Double click the **FireDrive** icon.
- Double click the **Mice** folder.
- Press **-N** on the keyboard to create a new folder.
- Name the new folder for the current mouse run:  
mm/dd/yy-n  
where n is the mouse number in the series  
e.g. **2/5/01-11**
- Double click the new folder.
- Create **event files**, **time cuts**, and **images** folders.

Launch Data Acquisition software:

- Double click icon labeled **Data Acquisition** with the correct combination of PSPMTs. A and B are the 5" tubes and C is the 1" tube.

Start data acquisition:

- Go to the **File** menu.
- Highlight **New**
- Highlight **Event File..**
- Select the current mouse's directory (which you created earlier).
- Double click the **event files** folder.
- Click **New Folder**.
- Type the name of the current run (dd/mm/yy-n-h) where it says Untitled. h represents the hour after injection imaging starts.
- Type the name of the current run (dd/mm/yy-n-h) where it says Untitled.
- Click **Save**.
- Click the button that looks like a disk with a small arrow pointing to it to turn on file saving.
- Click the right-hand arrow button.
- Click **OK** to load calibration files.
- Click **Start**.

Once the program has started collecting data, do not stop it until you have completed the run. Stopping and restarting during a run produces strange holes in the data. If there is a problem with the mouse, simply note the time to know later which time cut to ignore. The filename displayed in the upper right hand corner will change as the run progresses. Refer to the Troubleshooting section of these instructions if the computer freezes.

Stop data acquisition:

- Click the **Stop** button when the desired amount of time is up.
- Click the right-hand arrow button.
- Go to the **File** menu.
- Select **Close Write Event File**.
- Go to the **File** menu again.
- Select **Quit**.
- Click **No** when asked to save changes to Instrument.

## Take Data (Histograms)

Launch Data Acquisition software:

- Double click icon labeled **Data Acquisition** with the correct combination of PSPMTs. A and B are the 5" tubes and C is the 1" tube.

Start data acquisition:

- Click the right-hand arrow button.
- Click **OK** to load calibration files.
- Click **Start**.

Stop data acquisition:

- Click the **Stop** button when the desired amount of time is up.
- Click on the window with the image you wish to save. Generally this will be **A\_FULL**, **B\_FULL**, or **C\_FULL**.
- Go to the **File** menu.
- Highlight **Save**
- Select **Histogram As...**
- Select the correct Folder (date/images)
- Add date and number marker to highlighted name.
- Click **Save**.
- Repeat data acquisition as many times as desired.
- Click the right-hand arrow button.
- When finished, go to the **File** menu.
- Select **Quit**.
- Click **No** when asked to save changes to Instrument.

## Take Data (SPECT Histograms)

Launch Data Acquisition software:

- Double click icon labeled **Data Acquisition** with the correct combination of PSPMTs. A and B are the 5" tubes and C is the 1" tube.

Start data acquisition:

- Click the **Timer Preset** button.
- Enter desired time of runs in seconds (e.g. 3 minutes = 180).
- Click the right-hand arrow button.
- Click **OK** to load calibration files.
- Click **Start**.

Stop data acquisition:

- The program will automatically stop taking data when the correct amount of time is up. The **Stop** button will change back to **Start**.
- Click the **Start** button once the imaging angle has been changed.
- Click on the window with the image you wish to save. Generally this will be **A\_FULL**, **B\_FULL**, or **C\_FULL**.
- Go to the **File** menu.
- Highlight **Save**
- Select **Histogram As...**
- Select the correct Folder (date/images)
- Add degree marker to highlighted name.
- Click **Save**.
- When finished, click the right-hand arrow button.
- Go to the **File** menu.
- Select **Quit**.
- Click **No** when asked to save changes to Instrument.

## B. Data Analysis

### 1. Make Time Cuts

Transfer files from G3 to G4:

- Double click on the **FirePowerHDD** icon on the G4's desktop.
- If there is no icon:
  - Go to the Apple menu (top left of screen)
  - Click on the apple and pull down to **Network Browser**.
  - Click the arrow next to **AppleTalk**.
  - Click the arrow next to **Curie**.
  - Enter the password.
  - Double click **FirePowerHDD**.

Close the Network Browser by clicking the square in the upper left-hand corner of the window.

- Double click the mouse's folder you will make time cuts for.
- Double click on the **Mouse Data** folder on the G4's desktop.
- Press Apple-N on the keyboard to create a new folder.
- Type in mouse's name.
- Press **return** on the keyboard.
- Drag the **event files** folder from the FireDrive to the folder you just created on the G4.

Create necessary folders:

- Double click the **Mice Data** folder on the desktop.
- Double click the mouse's folder that you will make time cuts for.
- Press Apple-N on the keyboard to create a new folder.
- Type in **time cuts**.
- Double click the **time cuts** folder you just created.
- Press Apple-N on the keyboard to create a new folder.
- Type in the correct folder name: nn-hh D dtt
  - nn: mouse number
  - hh: hour after injection
  - D: detector letter
  - tt: delta time
  - (e.g. **18-0 A d10**)

Start software:

- Double click the **Make Time Cut Files** icon.
- Press **return** when asked to select preferences.
- Enter the desired start time  
(injection time + 10 min - image start time)
- Press **return** on the keyboard.
- Enter the desired length of time for each cut (delta time) and press **return**.

Make time cut files:

- Click the **Sort Event Files** button.
- Select the mouse's directory:  
From the top, pull down to **Desktop**.  
Double click **Mice Data**.  
Double click the mouse's folder.
- Double click the **event files** folder.
- Double click the folder for the chosen run.
- Highlight the first file in the folder (the one without a % in the name)
- Click **Open**.
- Choose folder to save detector A's files in:  
From the top, pull down to the mouse's directory.  
Double click **time cuts**.  
Double click folder for chosen run and detector (e.g. **18-0 A d10**).  
Type in mouse name and detector where it says **untitled** (e.g. **4/2/01-18-0 A**).
- Repeat for detector B.

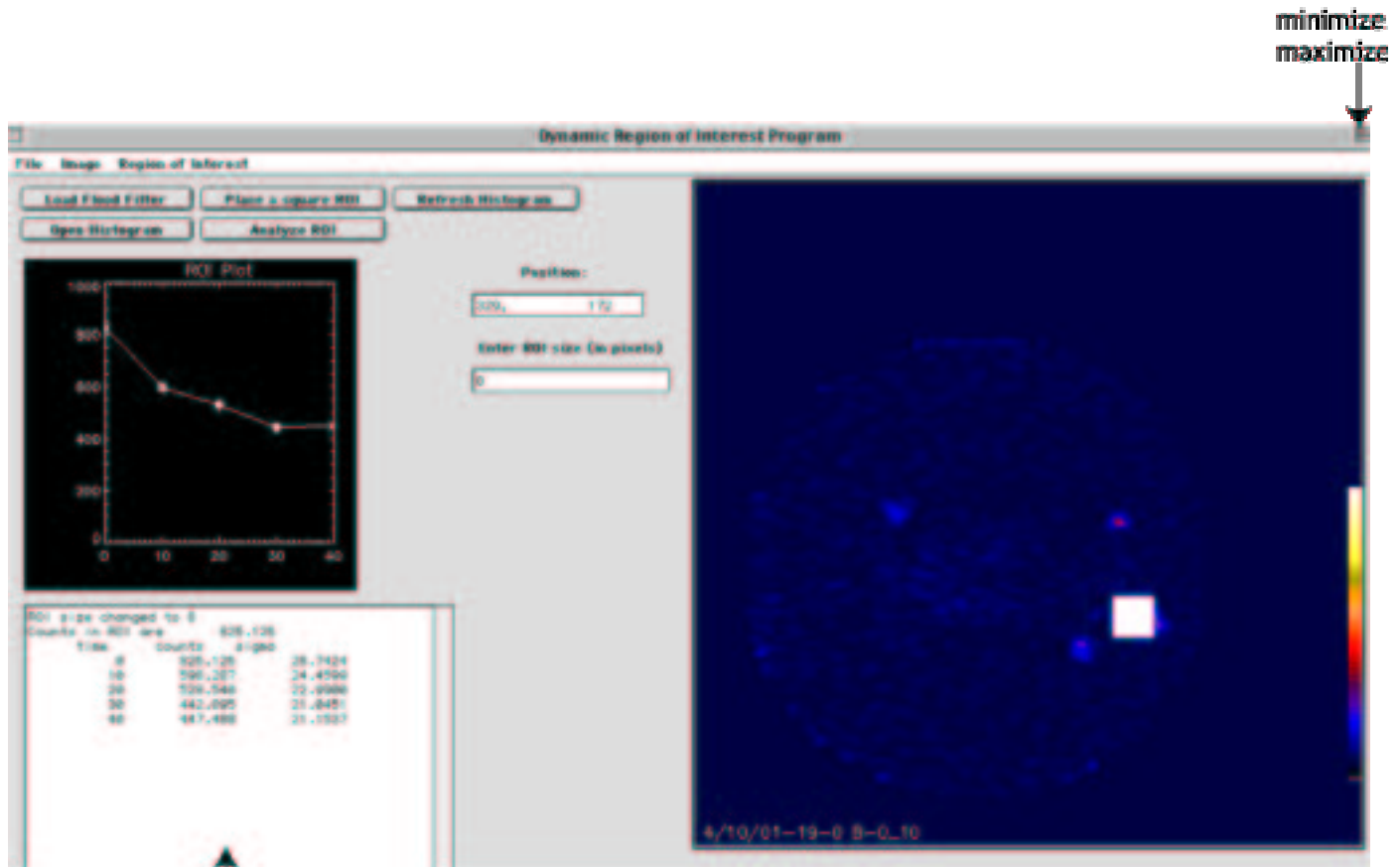
While the computer is making time cuts, the mouse pointer will be a watch. Once the program has finished, it will turn back to a normal pointer or cursor. Do not do anything else on the computer while it is making time cuts to reduce the risk of it freezing. Repeat the above steps until all desired runs have been made into time cuts.

It is important that the time cuts are stored in separate folders according to run as well as detector. If they are not, the analysis program will not work correctly. Also, the files will be saved with delta time markers added to the end of the file name, starting with zero (e.g. **4/2/01-18-0 A\_0-10**). When analyzing, add 10 min. to the times shown to get the time after injection.

## 2. Analyze Data

Start software:

- Double click the **Data Analysis** icon on the desktop.
- Press **return** on the keyboard to select the user preferences.
- Click the **Load Flood Filter** button.
- From the top, pull down to **Desktop**.
- Double click the **Mice Data** folder.
- Double click the **flood images** folder.
- Double click the correct file for either detector A or B.



report window  
Get image:

- Click the **Load Histogram** button.
- Click the **Desktop** button.
- Double click the **Mice Data** folder.
- Double click the desired mouse folder (e.g. **4/2/01-18**).
- Double click the **time cuts** folder.
- Double click the folder for the correct run and detector (e.g. **18-0 A d10**).
- Double click the file you wish to view (e.g. **4/2/01-18-0 A-50-60**).

If the background color is not blue or black, better images will be obtained if the color table is changed:

- Go to **Image**.
- Slide the **Stretch Bottom** marker until it is lined up with the current background color.
- Click **Done**.
- Minimize and the Maximize the IDL window to see the changes.

ROI analysis:

- To change the size of the ROI, enter the desired size and press **return** on the keyboard.
- Click the **Place a square ROI** button.
- Place the cursor over the middle of the region of interest.
- Click once.
  - A white square will appear and cover the area defined as the ROI.
  - The total number of counts in that region for that image are displayed in the report window.
- Click the **Analyze ROI** button.
  - The program will graph the counts in that region over the entire length of the run.
  - The values used to make the graph are displayed in the report window.

The text in the report window can be erased simply by highlighting it and pressing **delete** on the keyboard. The coordinates of the center of the last ROI placed will be displayed until the **Place a square ROI** button is clicked again and the cursor moved over the image. To get rid of the white squares, click the **Refresh Histogram** button.

You can open as many histograms from the same detector as you wish. If you want to switch detectors, however, you must quit and then restart the program in order to load a new flood image. There is currently no way to clear a loaded flood image, so trying to load another flood image, even the same one, without restarting will create errors.

## C. Making Composites

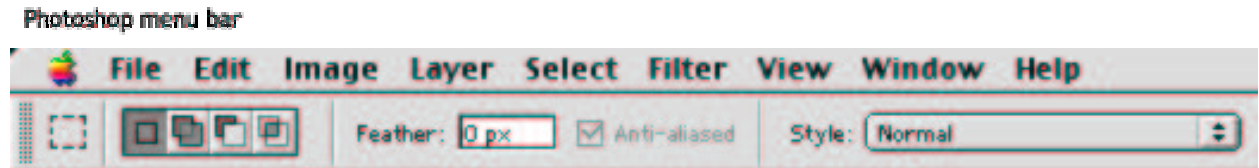
### 1. Make x-ray image

The x-ray shots from the analog camera are stored on the G3 in the Global Village file. These must be brought to the G4 for use. The files are automatically saved in consecutive order by date (e.g. Mar21\$26 = 26<sup>th</sup> image taken on March 21). Locate the series of images to be used (at present, all images have been moved to the G4 under the **mice images** folder).

The x-ray shots from the digital camera are stored in the **mice images** folder on the G4.

Open Photoshop.

- Go to **File**
- Go to **Open** (apple-O)
- Double click on each file to open. Each will tile in order ready for assembly in Photoshop.



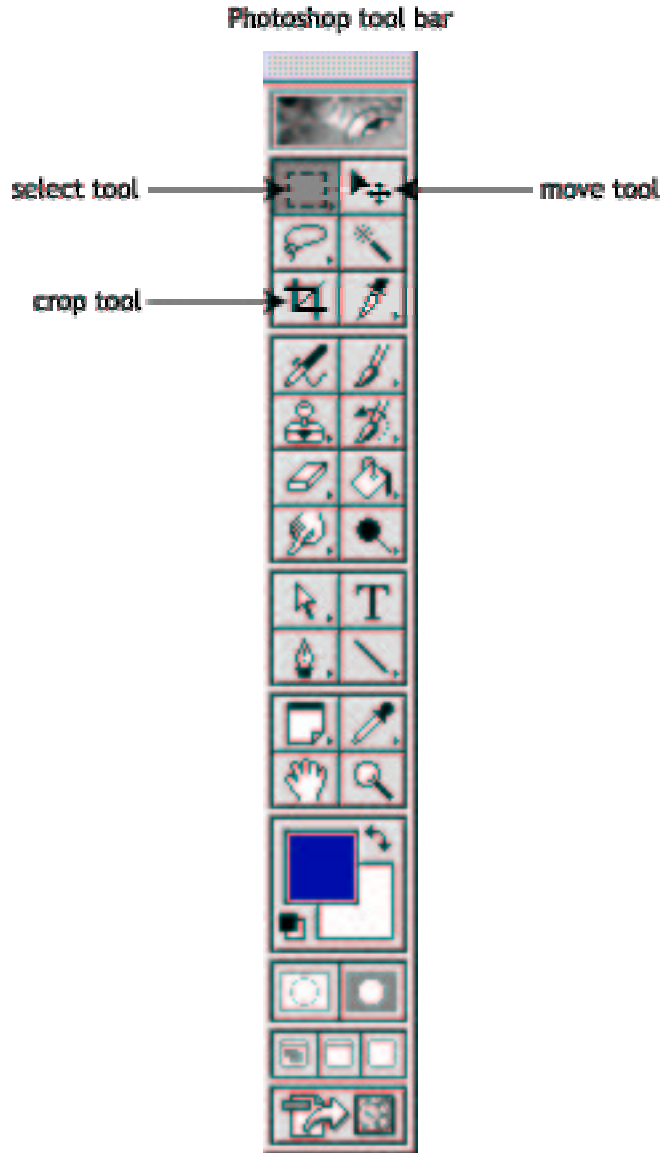
Create a New Page

- Go to **File**
- Select **New**

Go back to the tile of images and click to bring the first in the series to the front.

Adjust alignment and contrast:

- Go to **Image**
- Go to **Rotate Canvas**
- Select **90°** (CW or CCW so that the head is to the right)
  
- Go back to **Image**
- Go to **Adjust**
- Select **Auto Contrast**



Use the **select** tool to select the portion of the image for use.

Use Apple-C to copy the selection.

Click on the new blank page

Use Apple-V to paste the image on the new page.

Click on the **move** tool and use the mouse to move the image around on the new page.

Go back to the next image in the x-ray stack and click once to bring it to the front.

Repeat the **rotate**, **auto contrast**, and **select** a portion of the image for the next portion of the picture.

Repeat **copy**, click on the new page, and **paste** to the New Page.

Move the selection around with the **move** tool to align exactly with the first image. This alignment is facilitated by the thin diagonal wire embedded in the mouse bed.

When the entire image is constructed use the **crop** tool to size the full x-ray image.

Go to **Layer**

Select **Flatten Image** to remove all layers.

Go to **Save As** to save a .jpg file identified with the animal number and the hour of the image (e.g. x-ray 21-3.jpg).

Save this file in the correct mouse's

folder, under the **Mouse Data** folder. If this is the first image for the run, make a new folder titled **images** for these files.

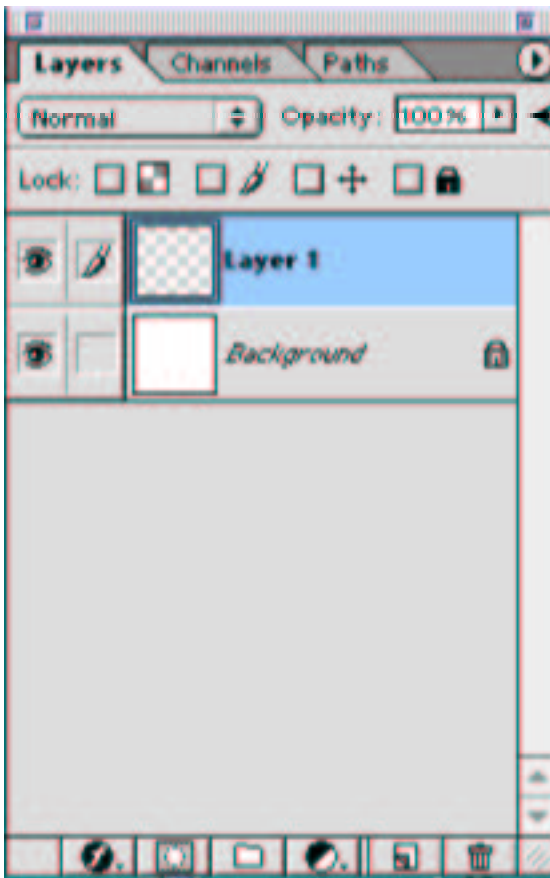
## 2. Co-register gamma image

To obtain the images of the gamma data double click the **Data Analysis** button on the Desktop.

Follow Data Analysis instructions to retrieve desired image.

Copy image from IDL to Photoshop:

- Click on the image to make it active
- Use the Apple-C command to copy the image
- Open Photoshop
- Use the Apple-V command to paste this image into a new Photoshop file that was made as described above.



**Copy** the x-ray image and then **paste** it in the middle of another new blank page (made as described above).

**Select** the corresponding area of the gamma image (as described for the x-ray reconstruction) and **copy** to the new page. Change the **opacity** of the gamma image layer from 100% to 50% in this step so that both images are seen.

Align the two views using the washers: the bright spots of activity on the gamma image are centered in the dark circles on the x-ray.

If necessary, adjust the **rotation** of the gamma image or the **size** of the x-ray image to obtain optimal alignment (see below for rotation and sizing instructions).

**Paste** another copy of the gamma image on the new page and position it above the co-registered images.

**Paste** another copy of the x-ray image on the new page and position it below the co-registered images.

Change the rotation of the gamma image:

- Go to **Image**
- Go to **Rotate Canvas**
- Select **Arbitrary...**
- Enter the desired degree of rotation, usually 3-6.
- Press **return** on the keyboard

Change the size of the x-ray image

- Go to **Image**
- Go to **Image Size...**
- Enter a new width, the height should change automatically
- Press **return** on the keyboard

Save and store the composite in the Image folder.

## REFERENCES

- [1] T. N. Aravantis, "Medical Imaging Techniques: Recent Advances and Applications," <http://www.cogs.susx.ac.uk/users/theoa/interactive/notes/medicalimagebgr.html> (1996).
- [2] N. Schramm, F. Sonnenberg, and H. Hallig, "Compact High Resolution Detector for Small Animal SPECT and the Scintigraphy of Human Extremities," *Zentrallabor fuer Elektronik* (1999).
- [3] Erik Stokstad, "Humane Science Finds Sharper and Kinder Tools," *Science* vol. 286, 1068 (1999).
- [4] M. B. Williams, V. Galbis-Reig, A. R. Goode, P. U. Simoni, S. Majewski, W. Phillips, and M. Stanton, "Multimodality Imaging of Small Animals," unpublished.
- [5] T. Mochizuki, V. L. Villemagne, U. Scheffel, X. Liu, J. L. Musachio, R. F. Daniels, and H. N. Wagner, Jr., "A simple probe measures the pharmacokinetics of [<sup>125</sup>I]RTI-55 in mouse brain in vivo," *European Journal of Pharmacology* vol. 338, 18 (1997).
- [6] Erik Stokstad, "Humane Science Finds Sharper and Kinder Tools," *Science* vol. 286, 1069 (1999).
- [7] Samuel Glasstone, Sourcebook on Atomic Energy (D. Van Nostrand company, Inc., Princeton, 1958) 2<sup>nd</sup> ed., p. 512.
- [8] T. McKee and J. R. McKee, Biochemistry: An Introduction (WCB/McGraw-Hill, Boston, 1999) 2<sup>nd</sup> ed., p. 100.
- [9] K. Ishizu *et al.*, "Ultra-high Resolution SPECT System Using Four Pinhole Collimators for Small Animal Studies," *The Journal of Nuclear Medicine* vol. 36 no. 12, 2282 (1995).
- [10] D. LeRoith, S. I. Taylor, and J. M. Olefsky, Diabetes Mellitus: A Fundamental and Clinical Text (Lippincott-Raven, Philadelphia, 1996) pp. 251-253.
- [11] M. W. Kalichman, "Diabetic Neuropathy," <http://medicine.ucsd.edu/neurosci/the-faculty/kalichman.html>.
- [12] T. McKee and J. R. McKee, Biochemistry: An Introduction (WCB/McGraw-Hill, Boston, 1999) 2<sup>nd</sup> ed., p. 455.
- [13] T. McKee and J. R. McKee, Biochemistry: An Introduction (WCB/McGraw-Hill, Boston, 1999) 2<sup>nd</sup> ed., p. 449.

- [14] D. Hargrove, "Research into Fat and Muscle Metabolism," <http://wciight.uams.edu/TNFresearch.htm> (University of Arkansas Medical Center).
- [15] T. N. Aravantis, "Medical Imaging Techniques: Recent Advances and Applications," <http://www.cogs.susx.ac.uk/users/theoa/interactive/notes/medicalimagebgr.html> (1996).
- [16] W. H. Brown and C. S. Foote, Organic Chemistry (Saunders College Publishing, Fort Worth, 1998) 2<sup>nd</sup> ed., pp. 463, 480.
- [17] T. N. Aravantis, "Medical Imaging Techniques: Recent Advances and Applications," <http://www.cogs.susx.ac.uk/users/theoa/interactive/notes/medicalimagebgr.html> (1996).
- [18] Samuel Glasstone, Sourcebook on Atomic Energy (D. Van Nostrand company, Inc., Princeton, 1958) 2<sup>nd</sup> ed., pp. 512-514.
- [19] Samuel Glasstone, Sourcebook on Atomic Energy (D. Van Nostrand company, Inc., Princeton, 1958) 2<sup>nd</sup> ed., pp. 527-528.
- [20] "Single-Photon Computed Tomography," Medical Imaging Techniques, <http://imasun.lbl.gov/~budinger/medTechdocs/PET.html>.
- [21] Samuel Glasstone, Sourcebook on Atomic Energy (D. Van Nostrand company, Inc., Princeton, 1958) 2<sup>nd</sup> ed., p. 181.
- [22] "Single-Photon Computed Tomography," Medical Imaging Techniques, <http://imasun.lbl.gov/~budinger/medTechdocs/PET.html>.
- [23] W. R. Leo, Techniques for Nuclear and Particle Physics Experiments (Springer-Verlag, Berlin, 1987), pp. 150, 157-158.
- [24] Eldon L. Keller, "Optimum Dimension of Parallel-hole, Multi-Aperture Collimators for Gamma-ray Cameras," vol. 9 no. 6, 233
- [25] M. F. Smith and R. J. Jaszczak, "The effect of gamma ray penetration on angle-dependent sensitivity for pinhole collimation in nuclear medicine," *Med. Phys.* vol. 24 no. 11, 1701 (1997).
- [26] Eldon L. Keller, "Optimum Dimension of Parallel-hole, Multi-Aperture Collimators for Gamma-ray Cameras," vol. 9 no. 6, 233
- [27] M. F. Smith and R. J. Jaszczak, "The Effect of Gamma Ray Penetration on Angle-dependent Sensitivity for Pinhole Collimation in Nuclear Medicine," *Med. Phys.* vol. 24 no. 11, 1702 (1997).

- [28] D. A. Weber and M Ivanovic, "Pinhole SPECT: Ultra-high Resolution Imaging for Small Animal Studies," *The Journal of Nuclear Medicine* vol. 36 no. 12, 2287 (1995).
- [29] W. R. Leo, Techniques for Nuclear and Particle Physics Experiments (Springer-Verlag, Berlin, 1987), pp. 169, 173.
- [30] A. G. Weisenberger, "Gamma-ray Imaging Detector for Small Animal Research," Ph.D. dissertation, College of William and Mary, 1998, p. 3.
- [31] M. F. Smith, D. R. Gilland, R. E. Coleman, and R. J. Jaszczak, "Quantitative Imaging of Iodine-131 Distribution in Brain Tumors with Pinhole SPECT: A Phantom Study," *The Journal of Nuclear Medicine* vol. 39 no. 5, 857 (1998).
- [32] Samuel Glasstone, Sourcebook on Atomic Energy (D. Van Nostrand company, Inc., Princeton, 1958) 2<sup>nd</sup> ed., pp. 298-300.
- [33] Samuel Glasstone, Sourcebook on Atomic Energy (D. Van Nostrand company, Inc., Princeton, 1958) 2<sup>nd</sup> ed., pp. 195-196, 306.
- [34] Photomultiplier Tubes and Assemblies, Hamamatsu Photonics K.K., Electron Tube Center (<http://www.hamamatsu.com>), pp. 3-4.
- [35] A. G. Weisenberger, "Gamma-ray Imaging Detector for Small Animal Research," Ph.D. dissertation, College of William and Mary, 1998, p. 69.
- [36] N. Schramm, F. Sonnenberg, and H. Hallig, "Compact High Resolution Detector for Small Animal SPECT and the Scintigraphy of Human Extremities," *Zentrallabor fuer Elektronik* (1999).
- [37] W. R. Leo, Techniques for Nuclear and Particle Physics Experiments (Springer-Verlag, Berlin, 1987), pp. 310, 313, 328.
- [38] R. Saunders, "Development of a Gamma Camera Array for Biological Imaging in Small Animal Research," thesis, College of William and Mary, 2000, pp. 22-23.
- [39] Photomultiplier Tubes and Assemblies, Hamamatsu Photonics K.K., Electron Tube Center (<http://www.hamamatsu.com>), pp. 4, 12.
- [40] L. G. Brown, "A Survey of Image Registration Techniques," (<http://www.researchindex.org>), pp. 4, 10.
- [41] M. B. Williams, V. Galbis-Reig, A. R. Goode, P. U. Simoni, S. Majewski, W. Phillips, and M. Stanton, "Multimodality Imaging of Small Animals," unpublished.